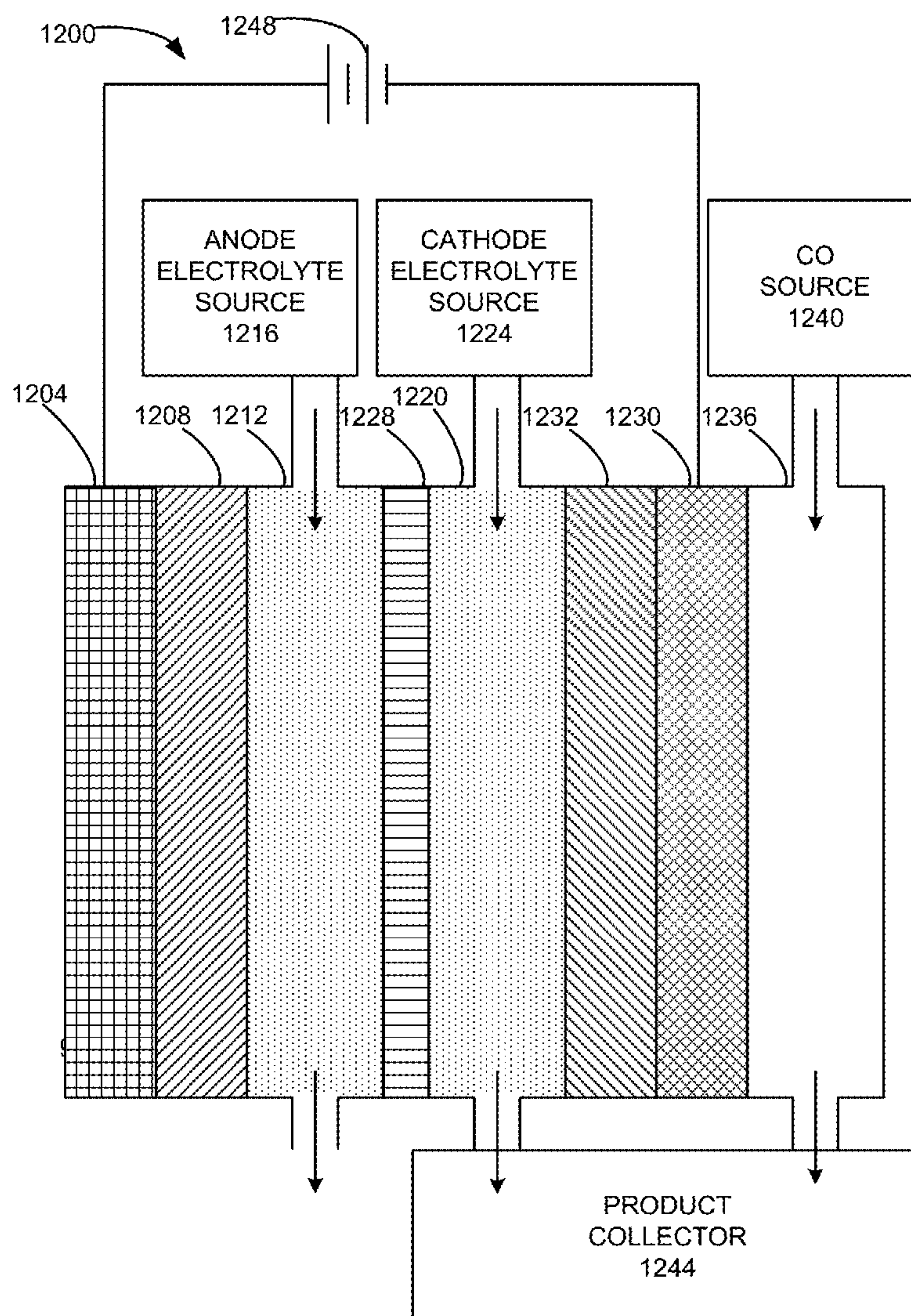


US 20150136613A1

(19) **United States**(12) **Patent Application Publication**
LI et al.(10) **Pub. No.: US 2015/0136613 A1**(43) **Pub. Date: May 21, 2015**(54) **CATALYSTS FOR LOW TEMPERATURE
ELECTROLYTIC CO REDUCTION****Publication Classification**(71) Applicant: **The Board of Trustees of the Leland
Stanford Junior University**, Palo Alto,
CA (US)(72) Inventors: **Christina LI**, Palo Alto, CA (US);
Matthew W. KANAN, Palo Alto, CA
(US)(21) Appl. No.: **14/604,198**(22) Filed: **Jan. 23, 2015****Related U.S. Application Data**(63) Continuation of application No. PCT/US2013/
025791, filed on Feb. 12, 2013.(51) **Int. Cl.**
C25B 1/00 (2006.01)
C25B 9/06 (2006.01)
(52) **U.S. Cl.**
CPC **C25B 1/00** (2013.01); **C25B 9/06** (2013.01)(57) **ABSTRACT**

A method for electrochemically reducing CO is provided. A cathode is provided, wherein the cathode comprises a conductive substrate with a catalyst of a metal and a metal oxide based coating on a side of the cathode. An anode is spaced apart from the cathode. An ionic transport is provided between the anode and cathode. The cathode is exposed to CO and H₂O. The anode is exposed to H₂O. A voltage is provided between the cathode and anode.



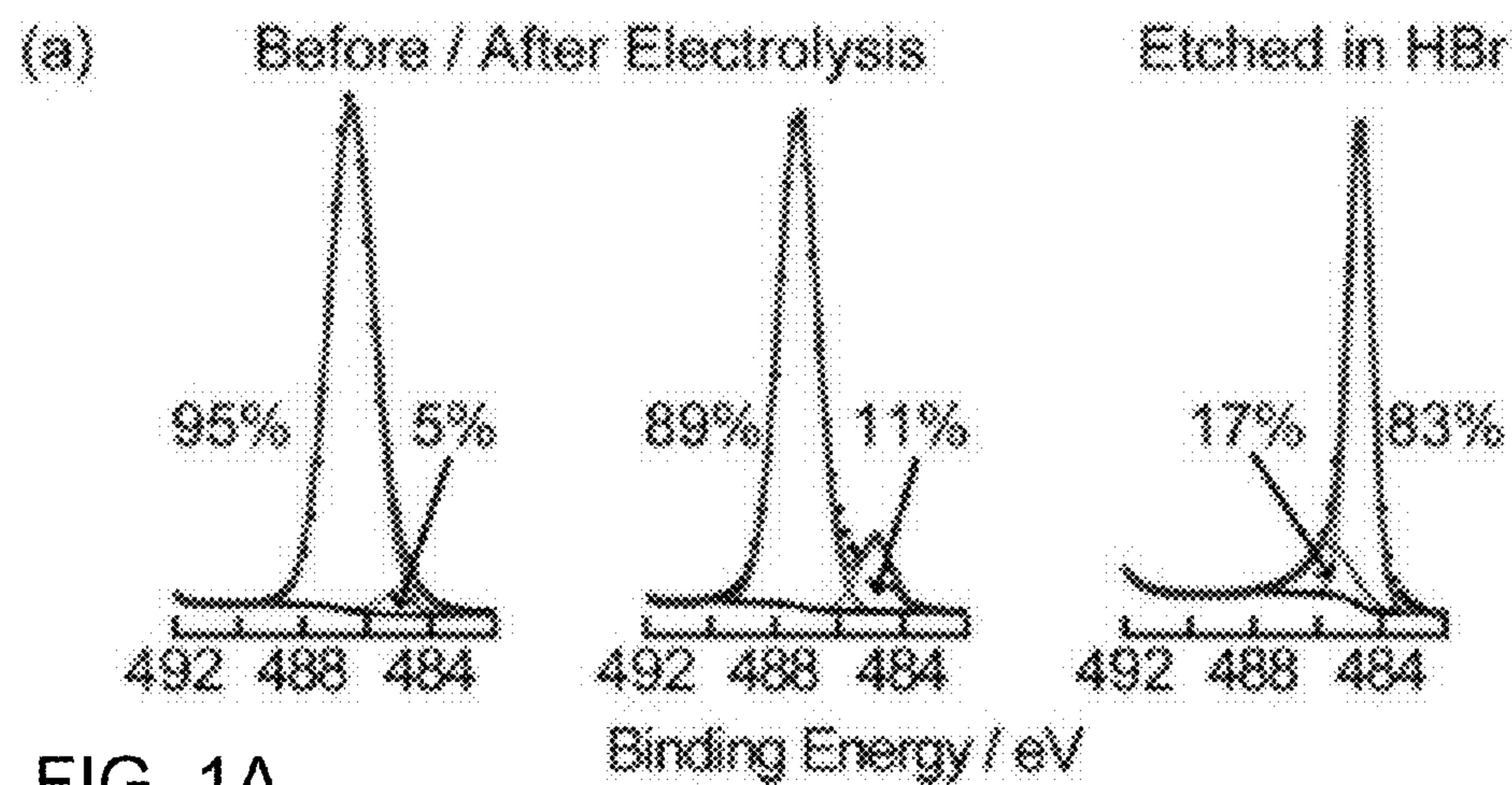


FIG. 1A

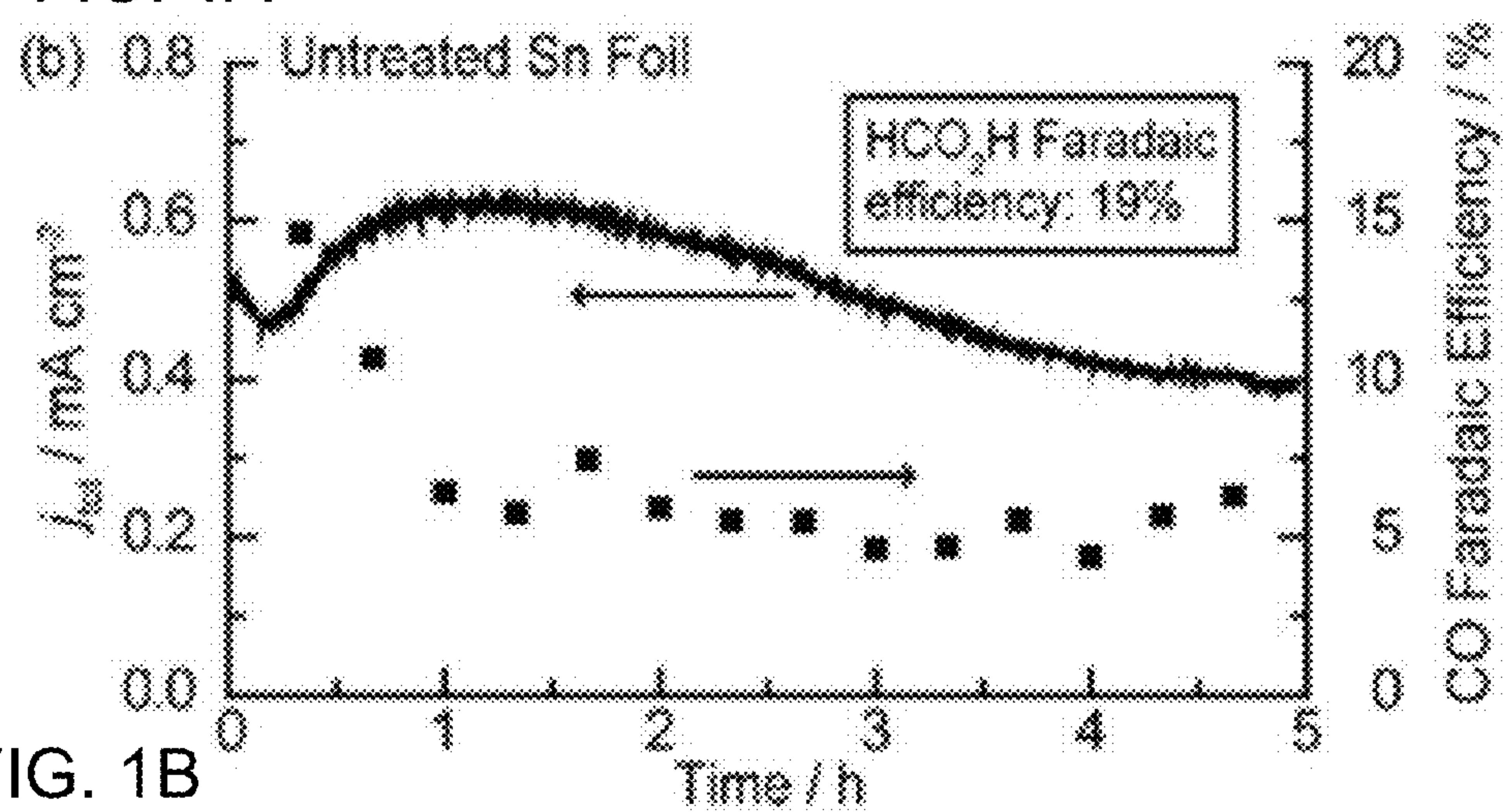


FIG. 1B

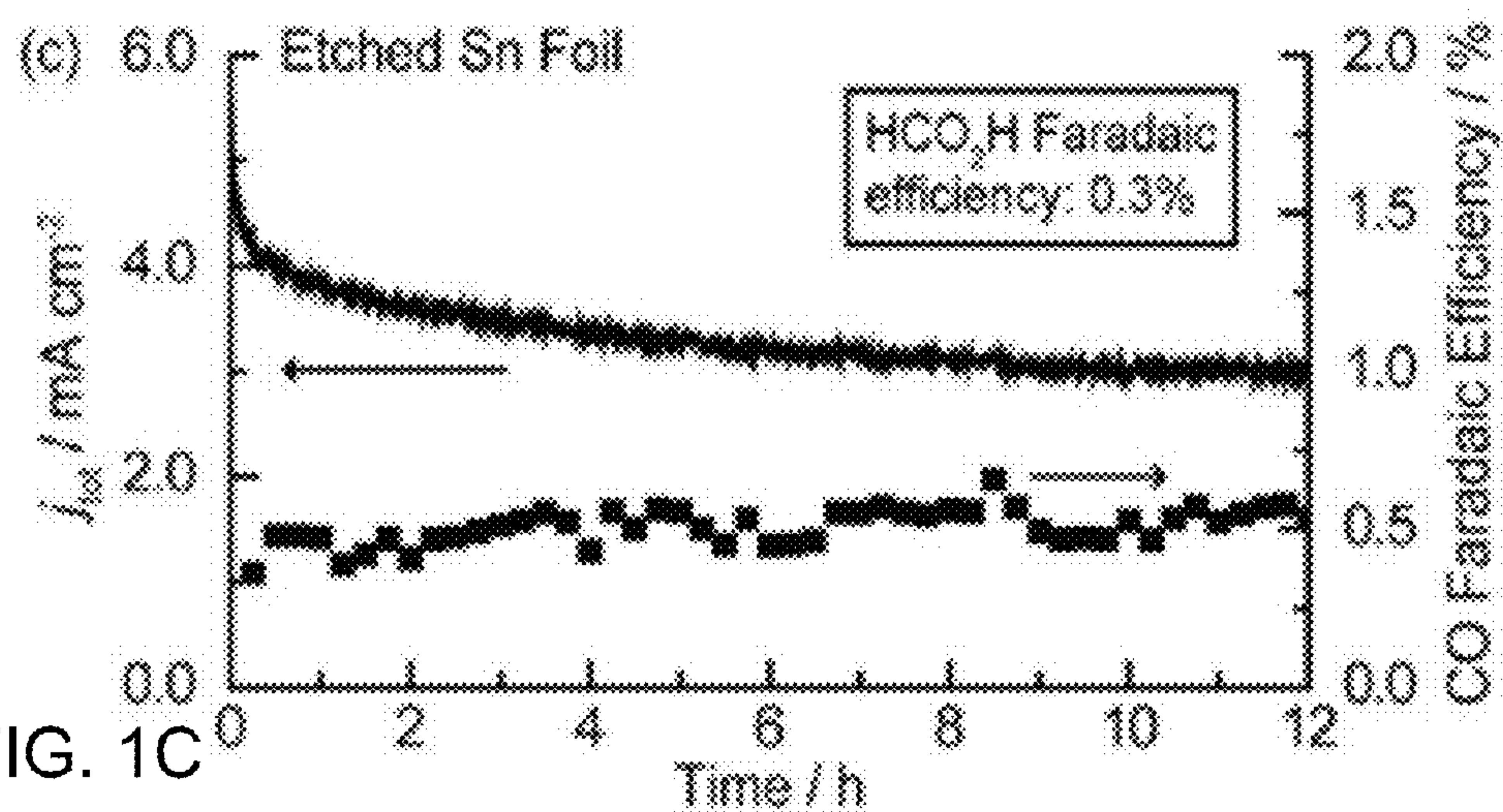


FIG. 1C

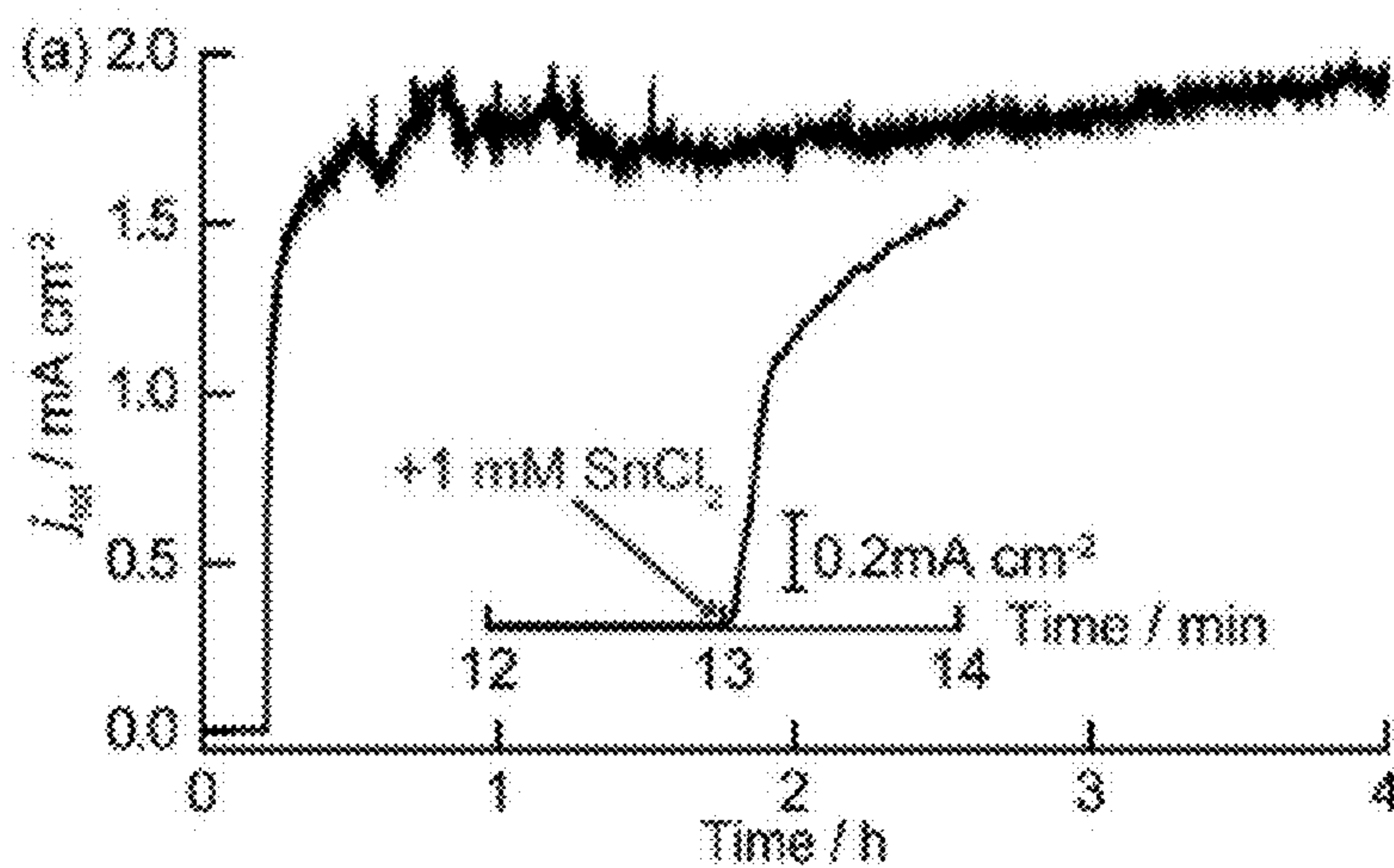


FIG. 2A

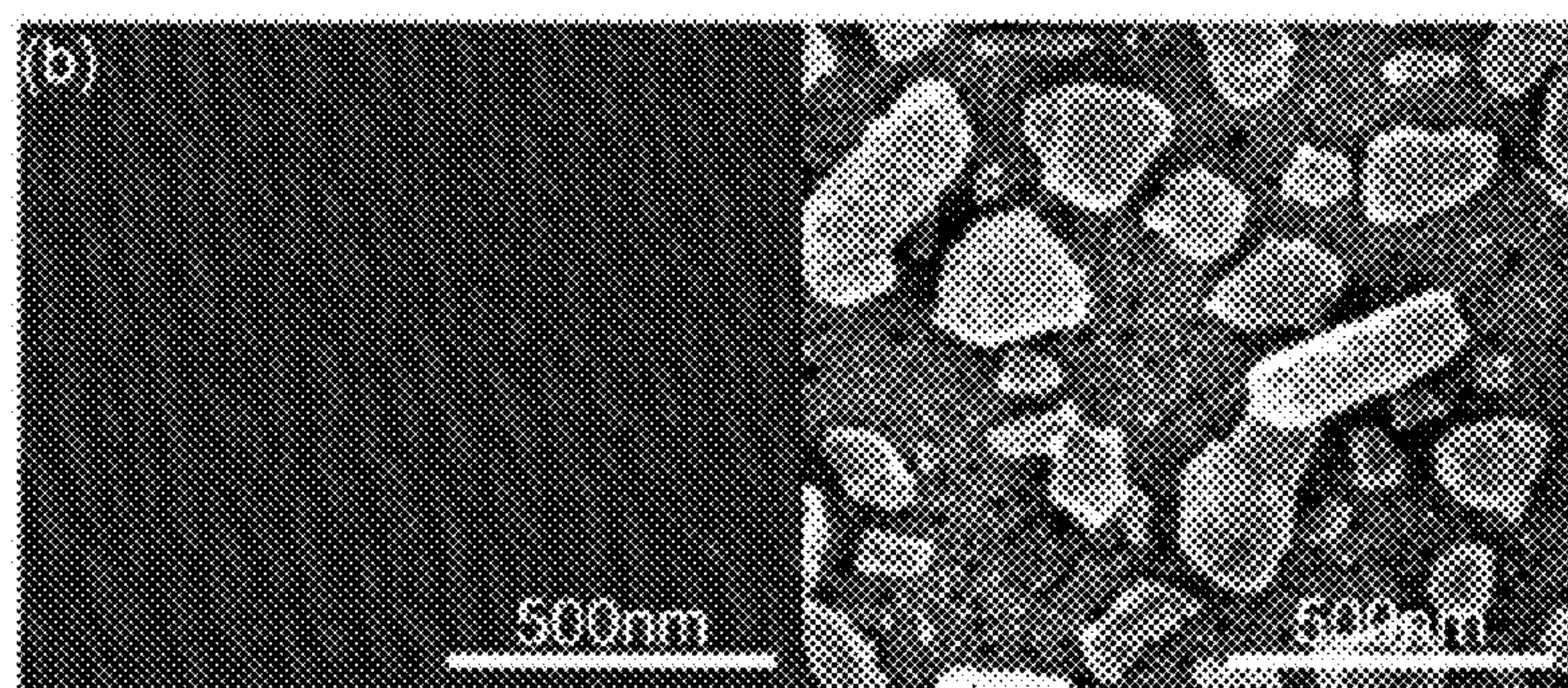


FIG. 2B

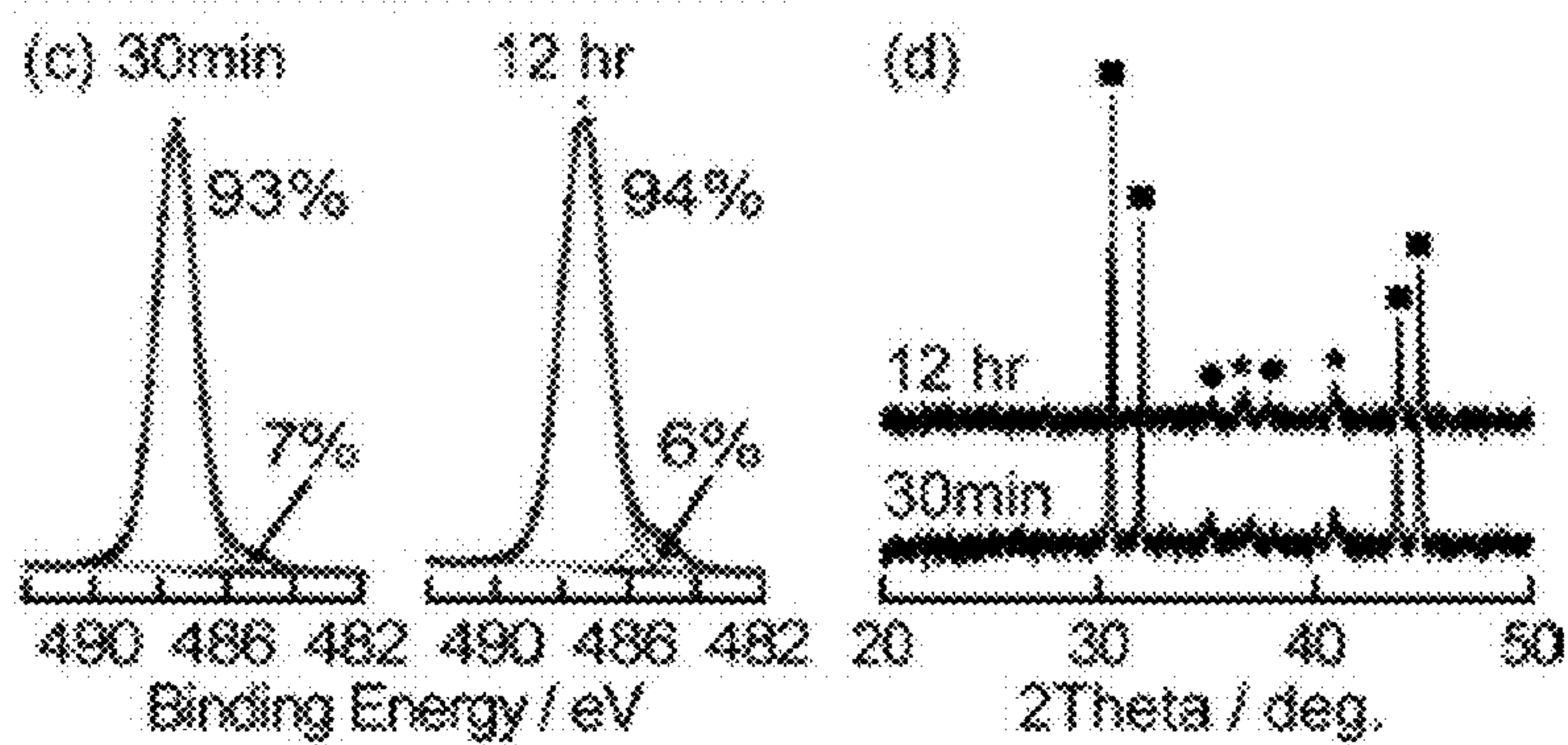
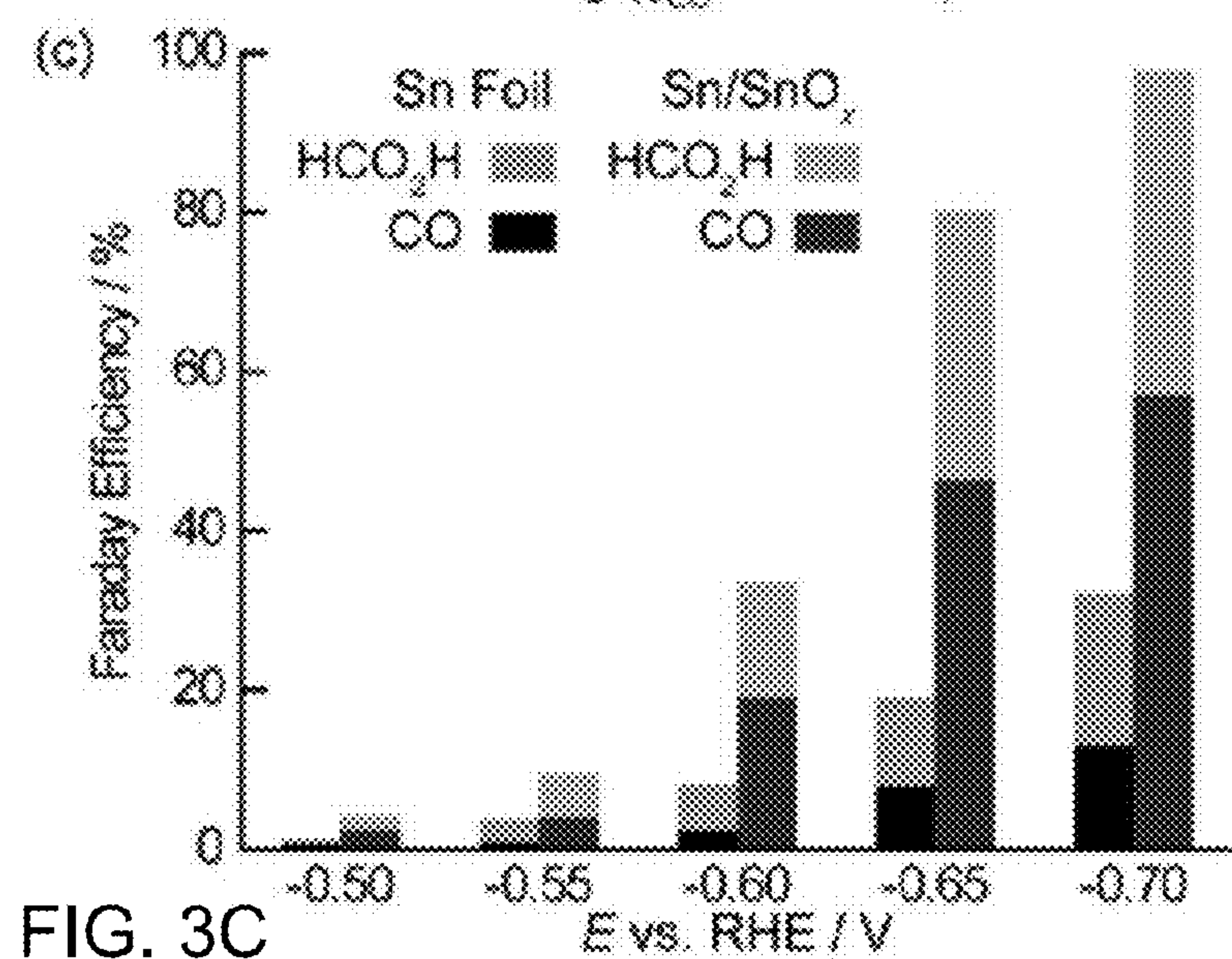
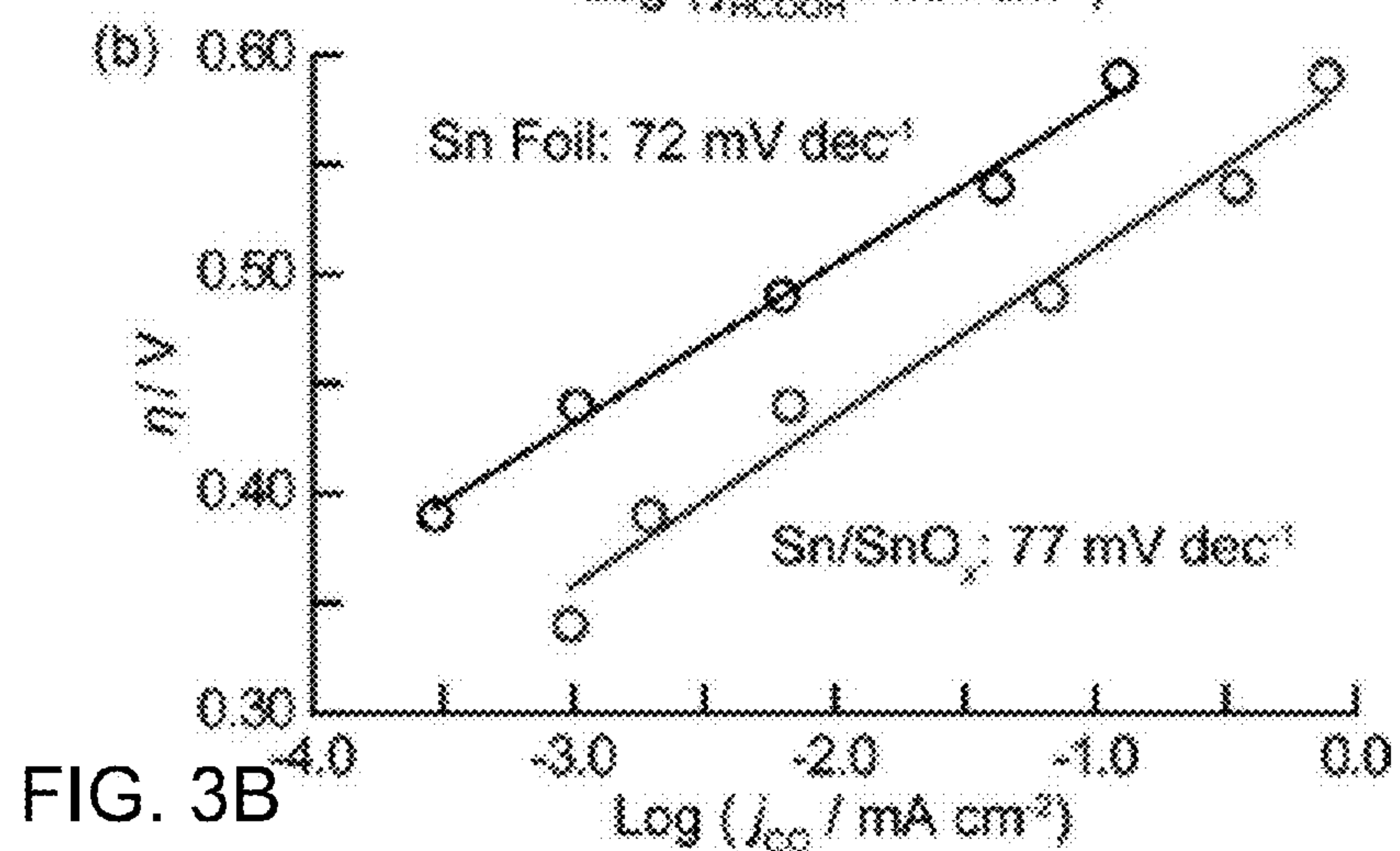
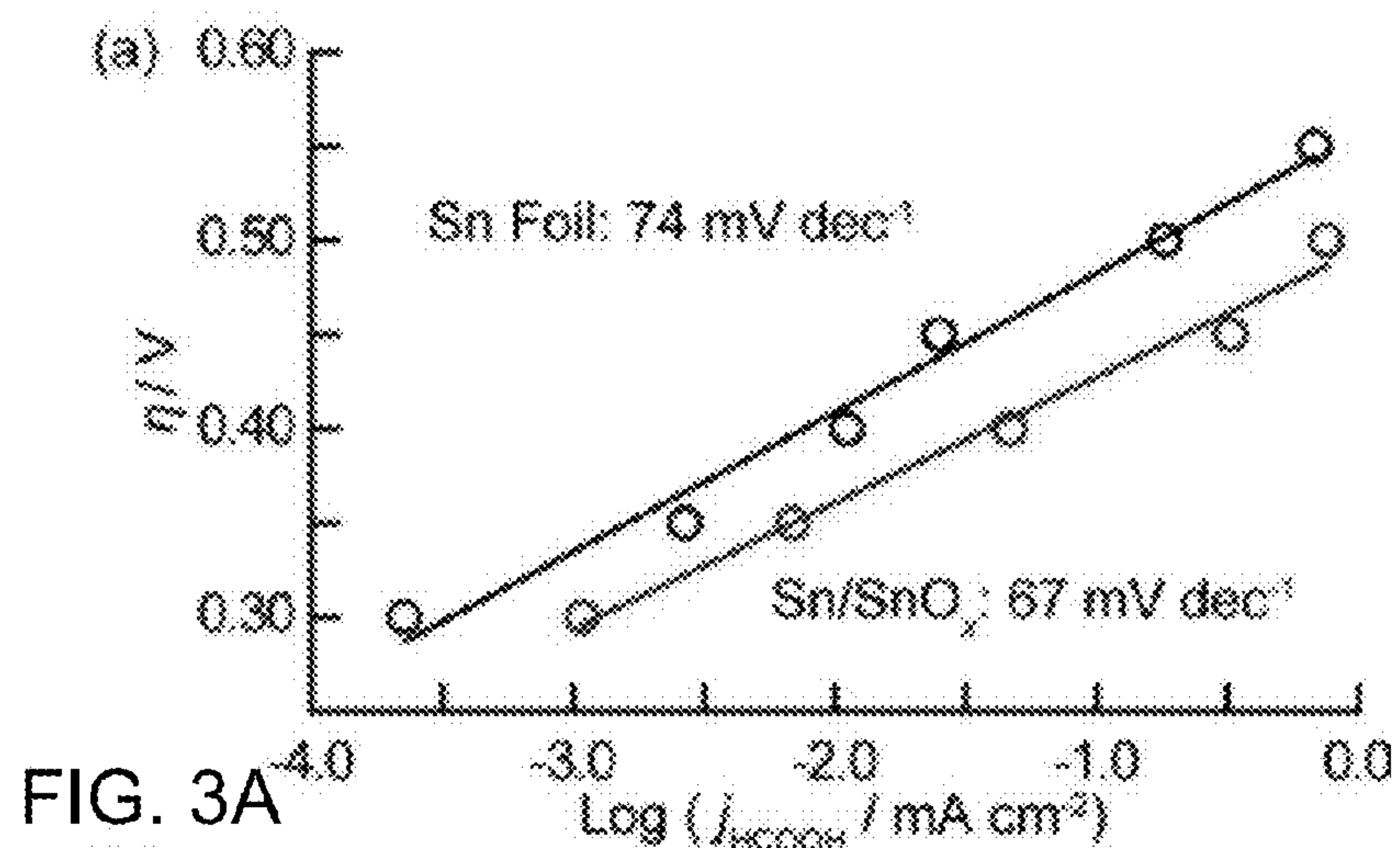


FIG. 2C

FIG. 2D



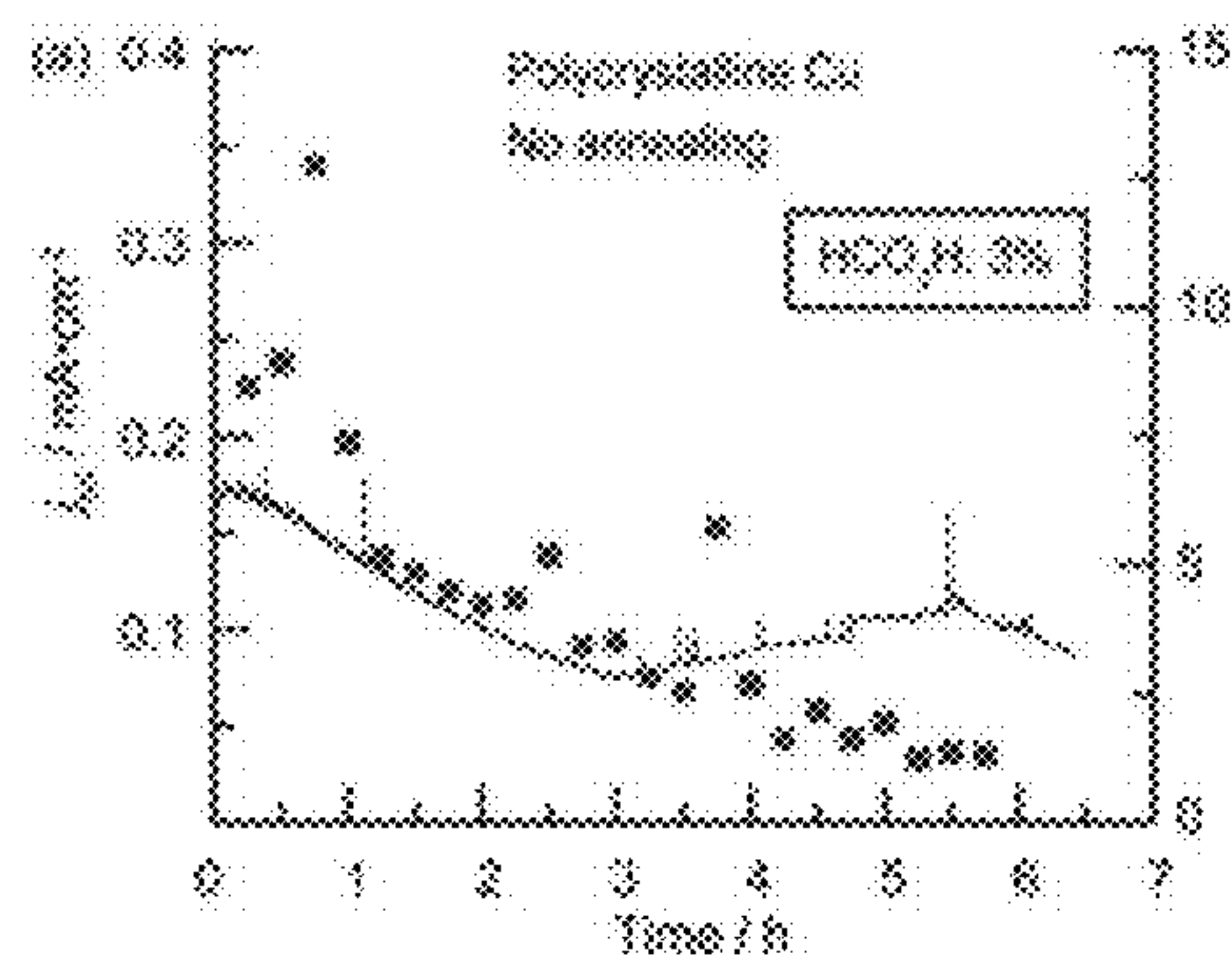


FIG. 4A

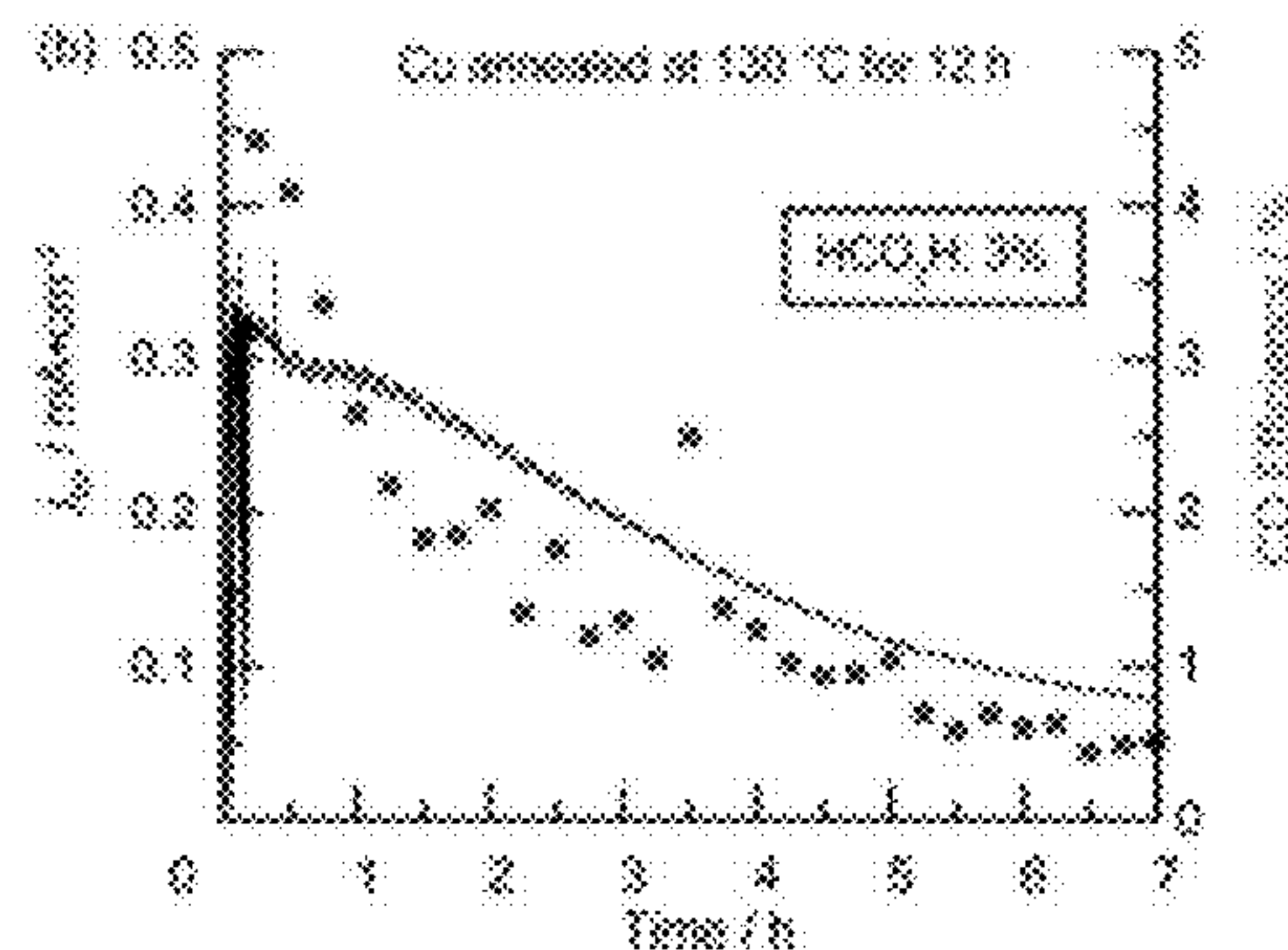


FIG. 4B

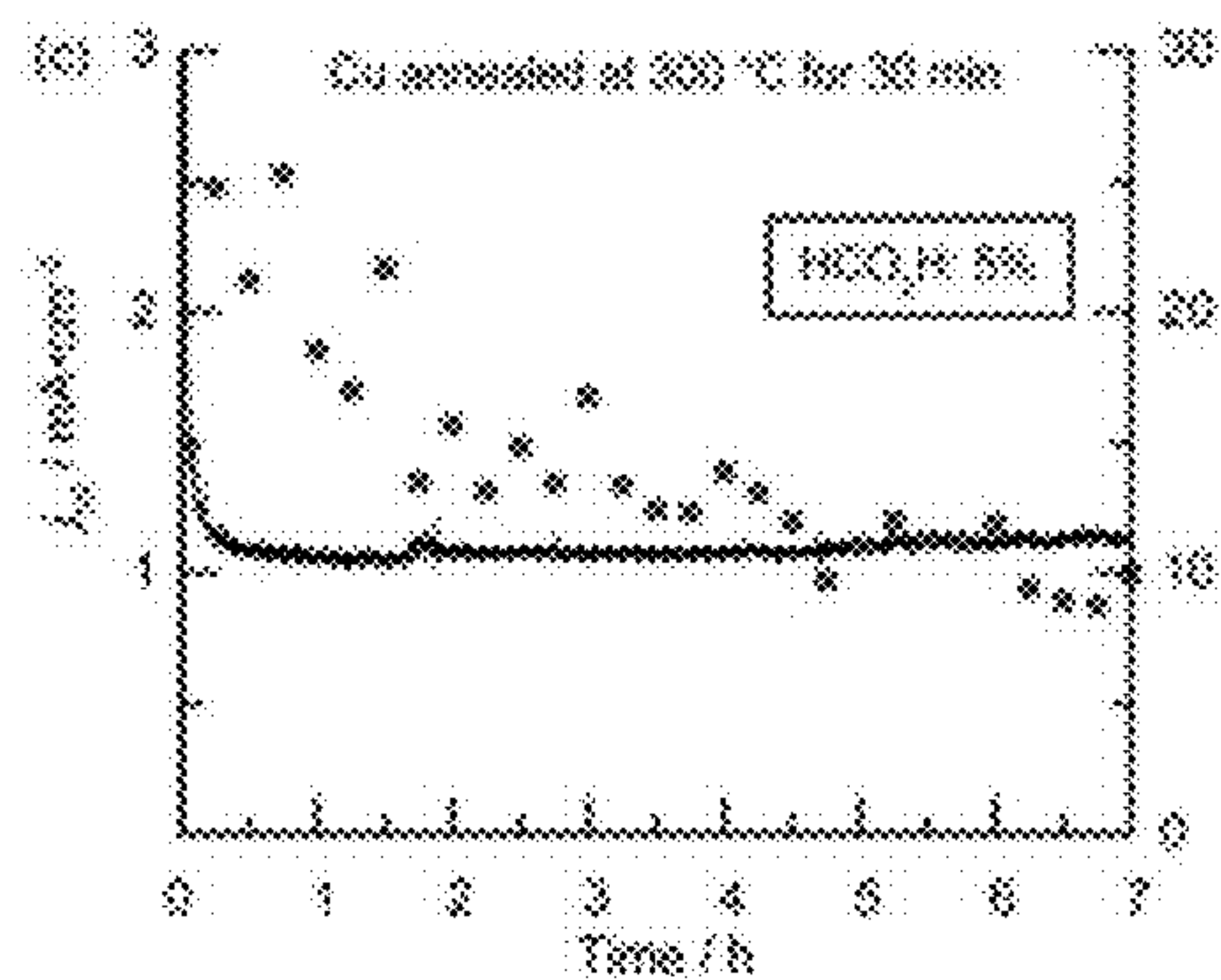


FIG. 4C

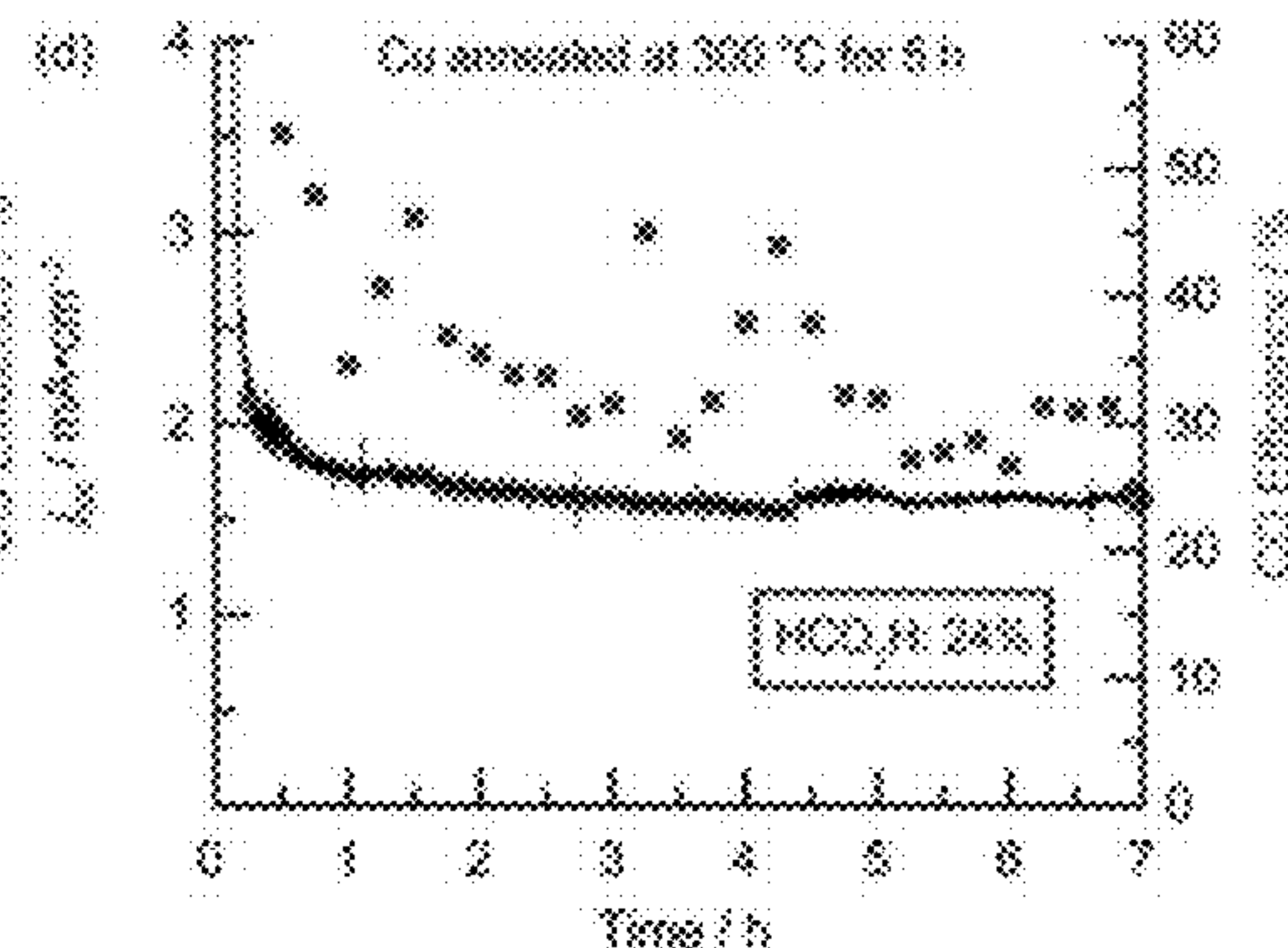


FIG. 4D

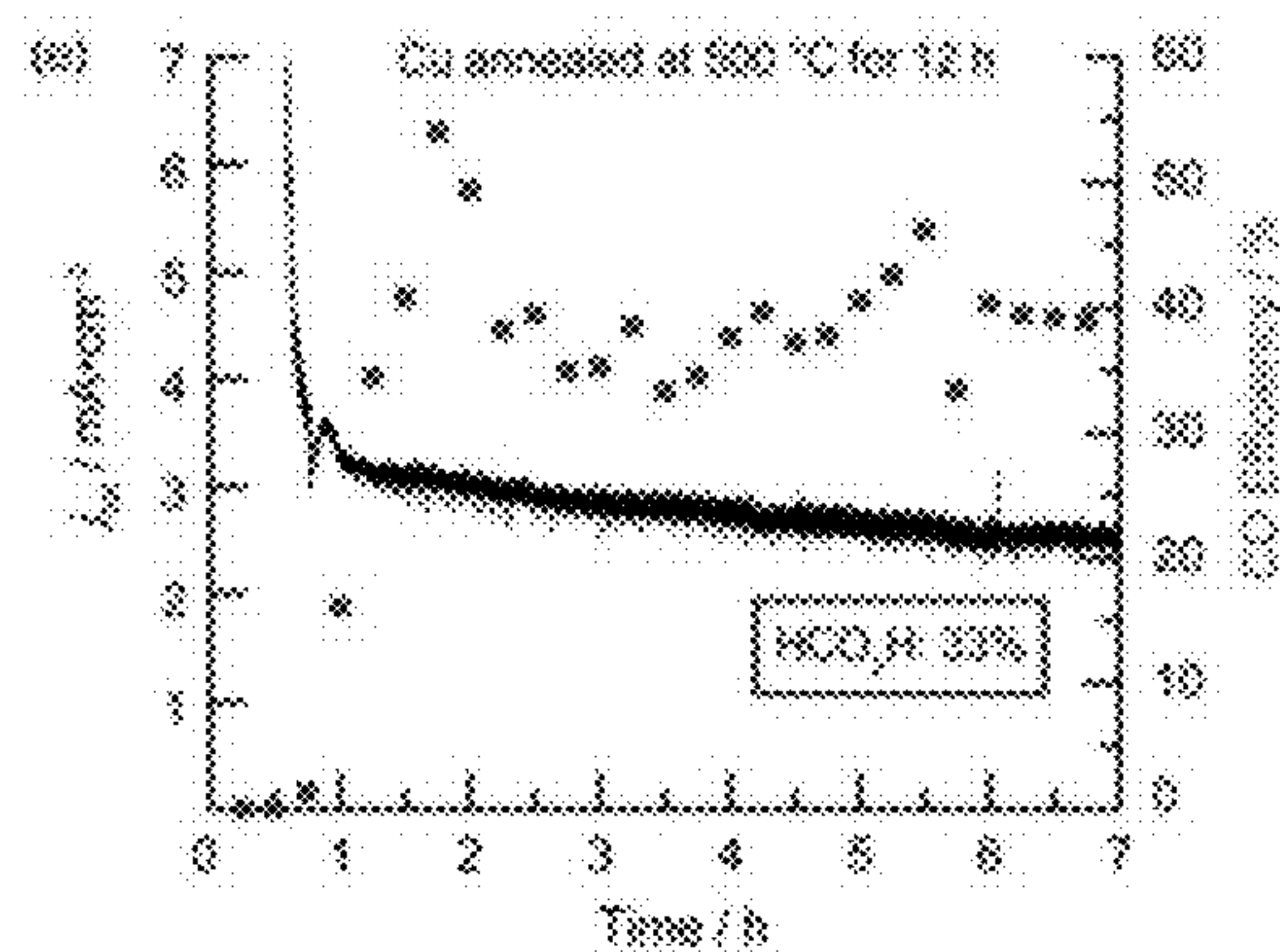


FIG. 4E

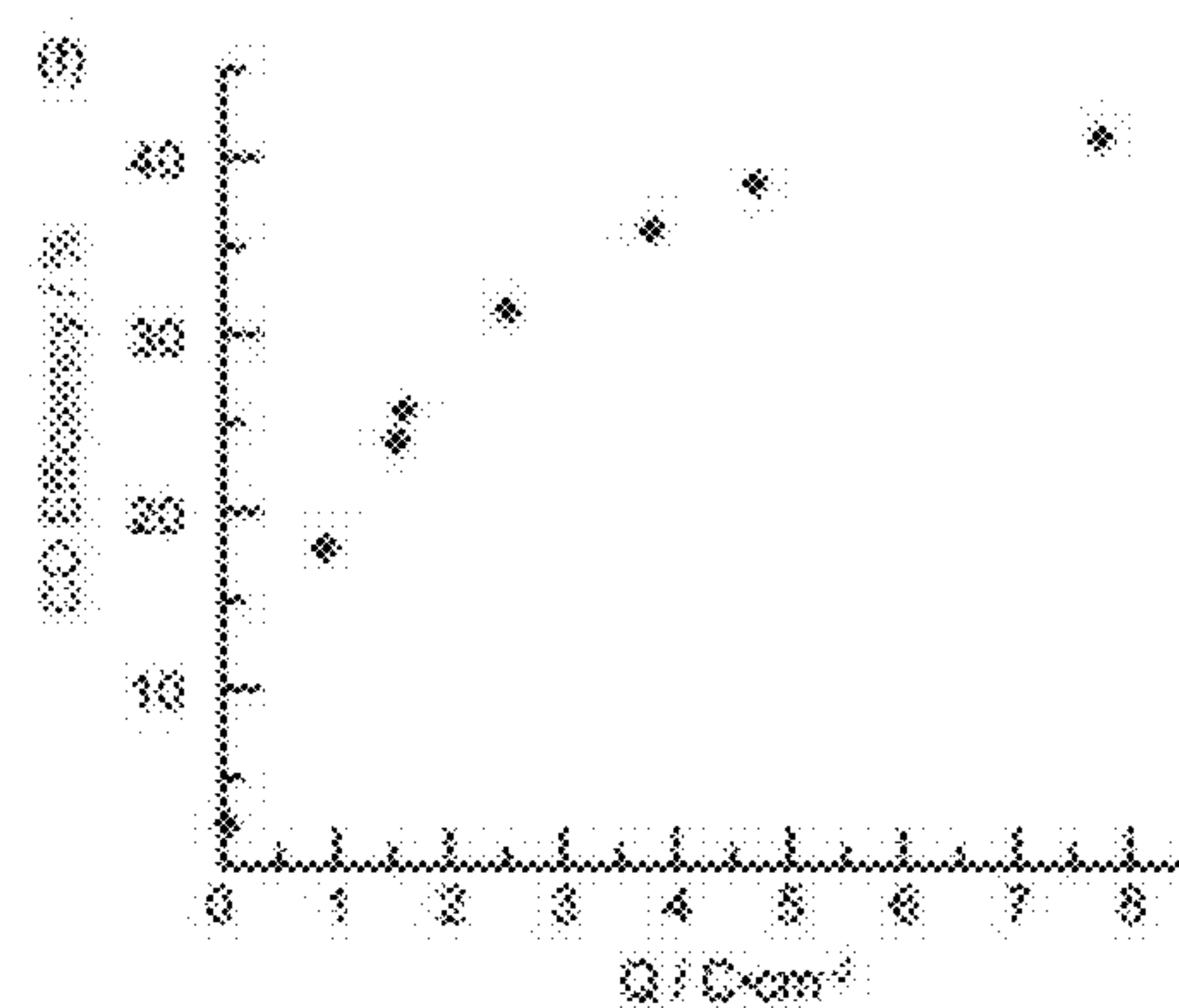


FIG. 4F

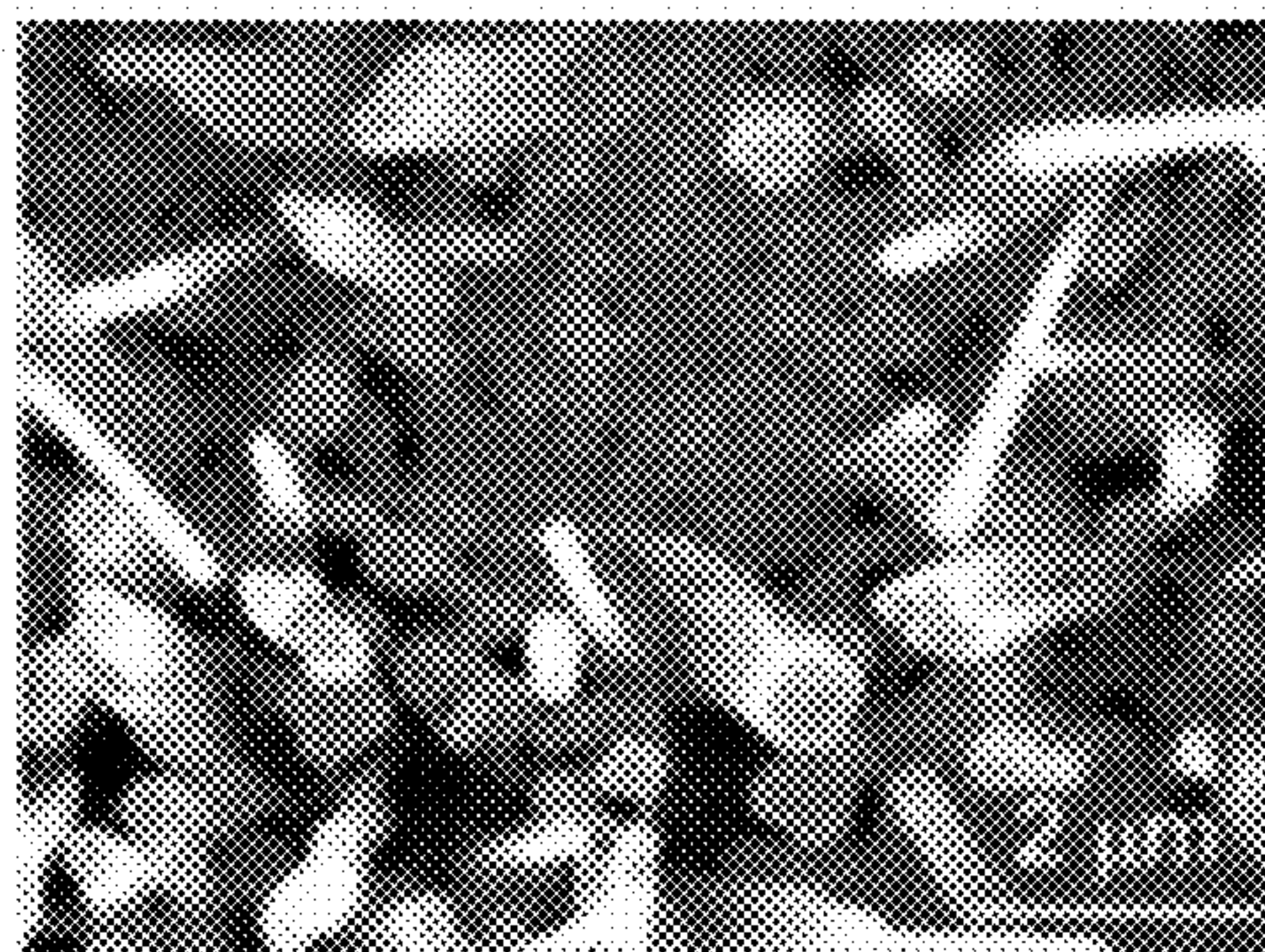


FIG. 5A

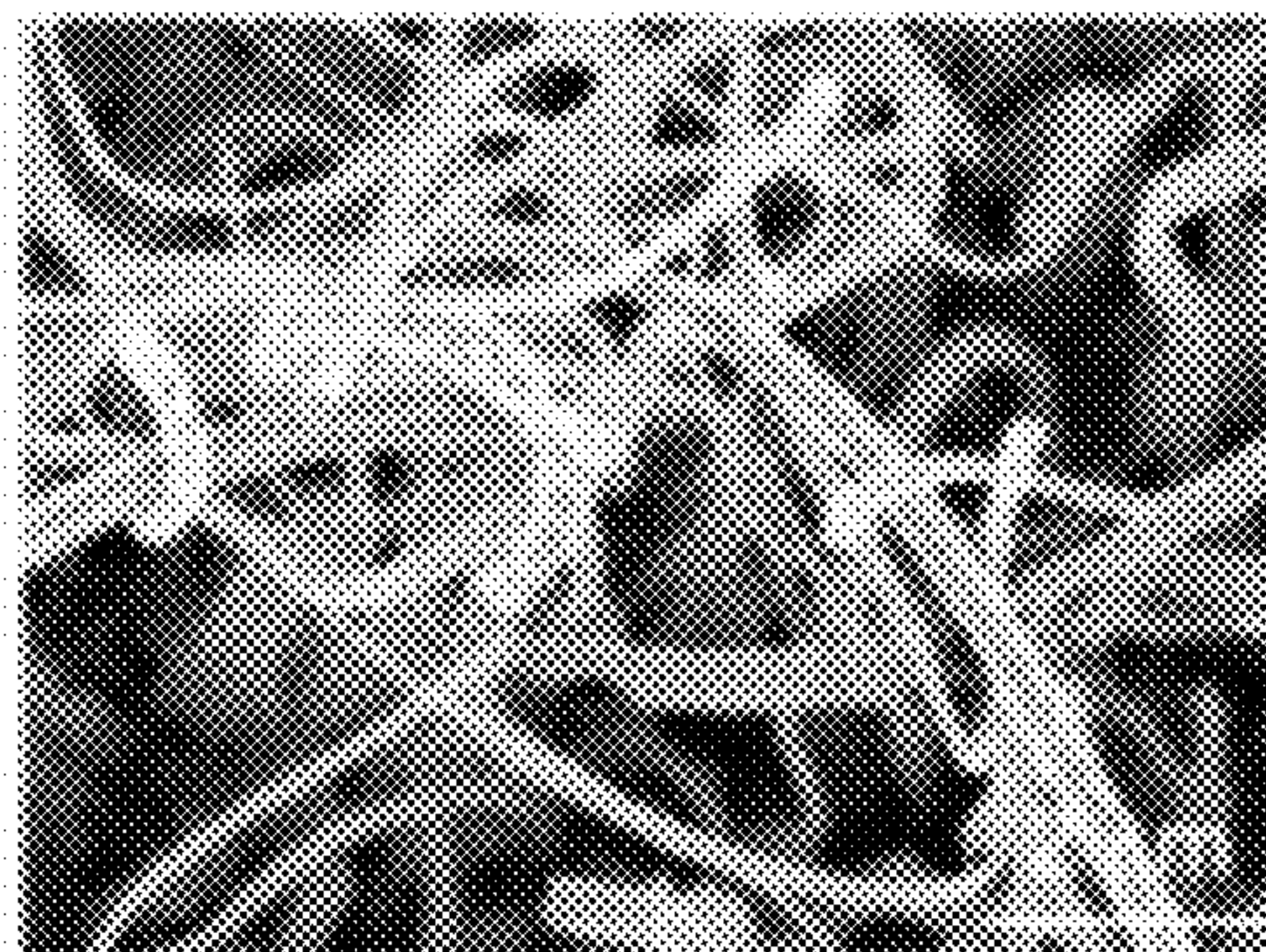


FIG. 5D

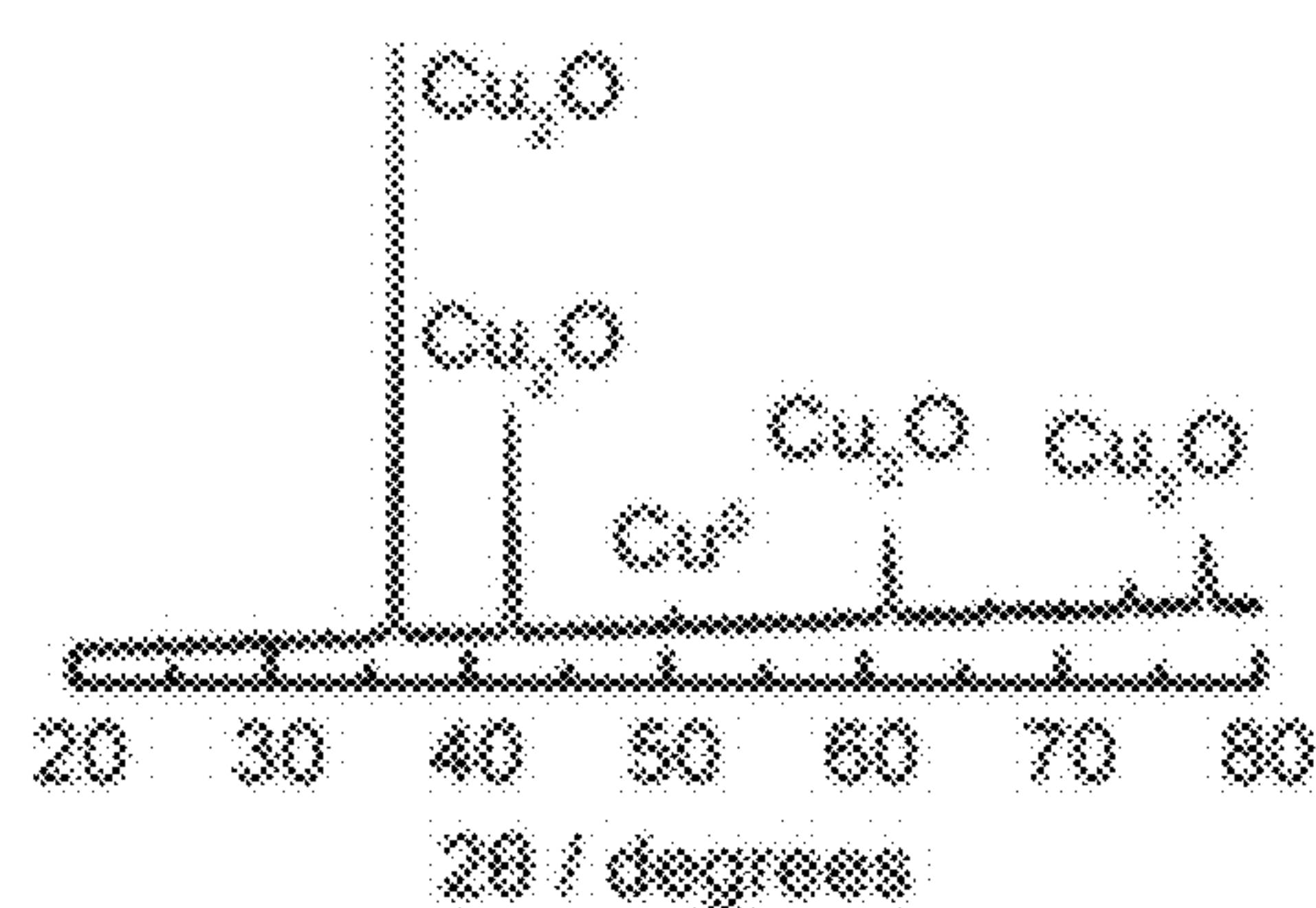


FIG. 5B

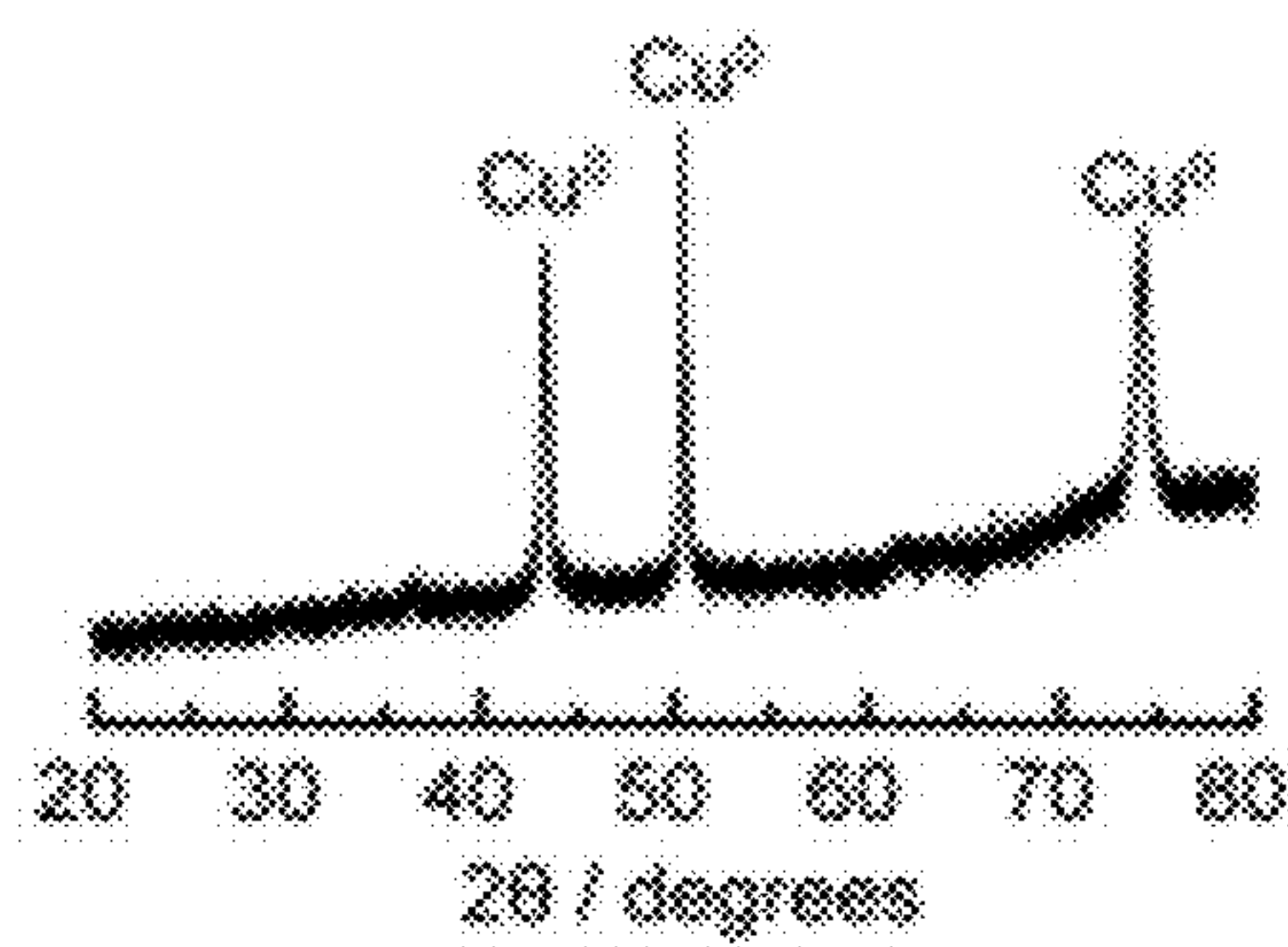


FIG. 5E

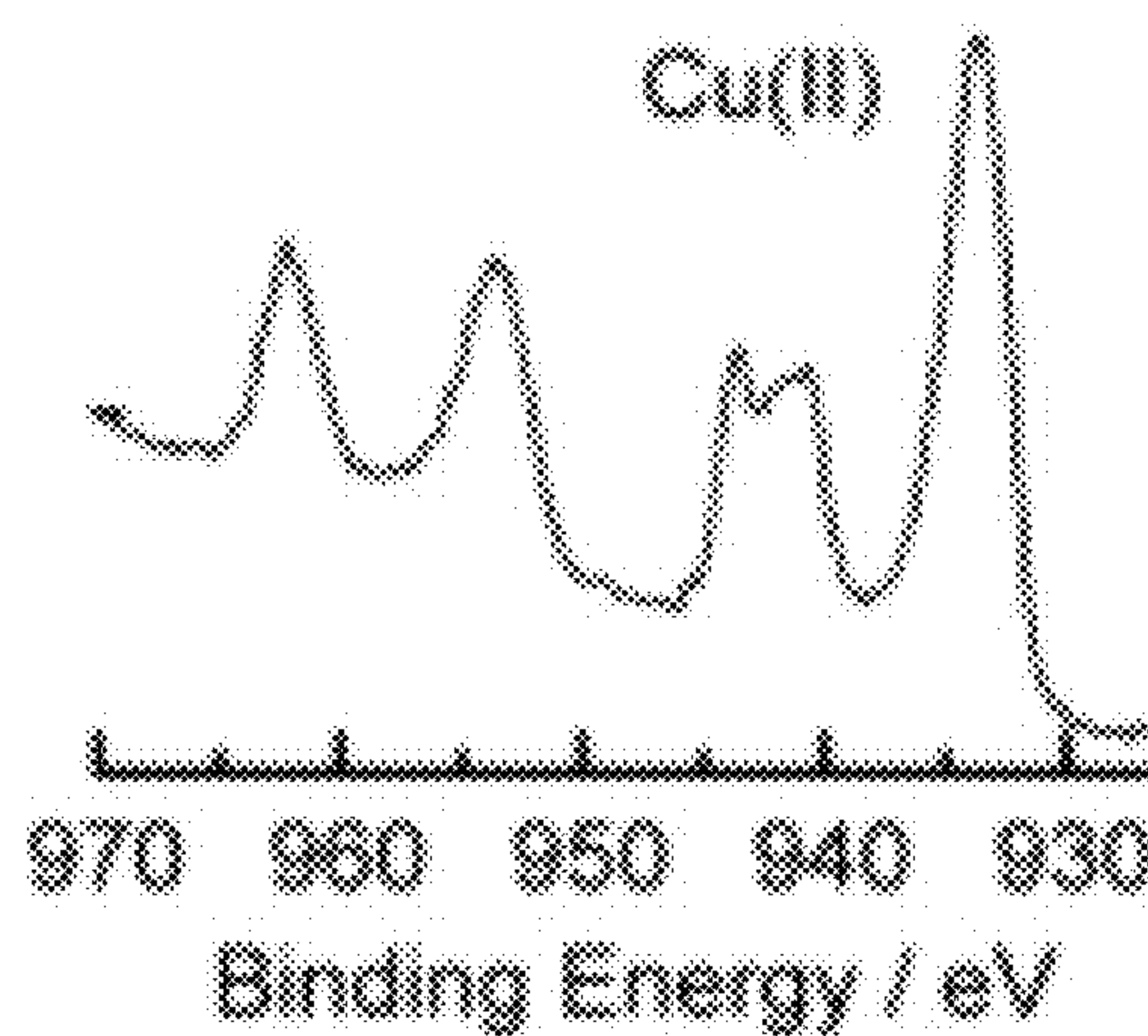


FIG. 5C

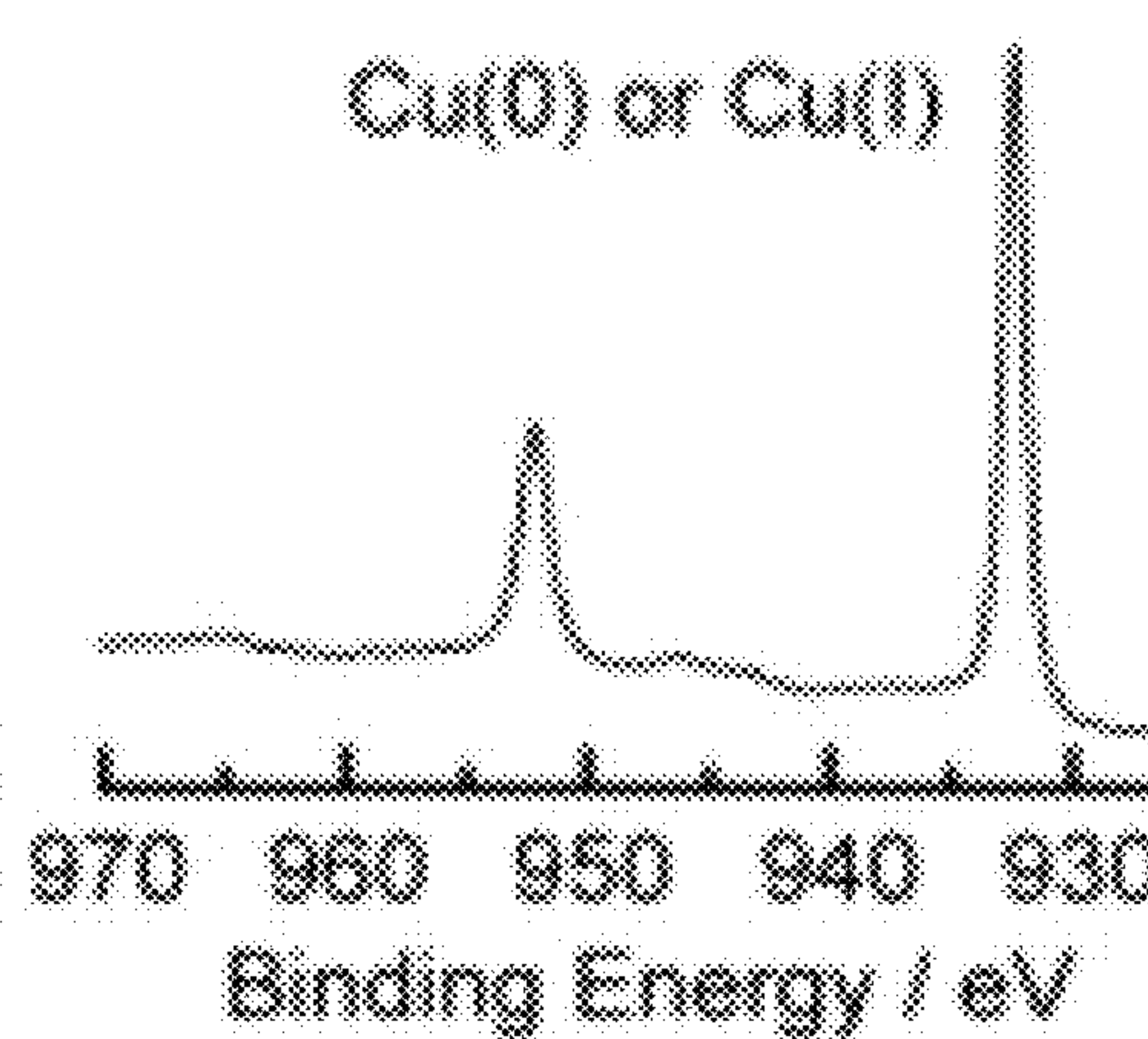


FIG. 5F

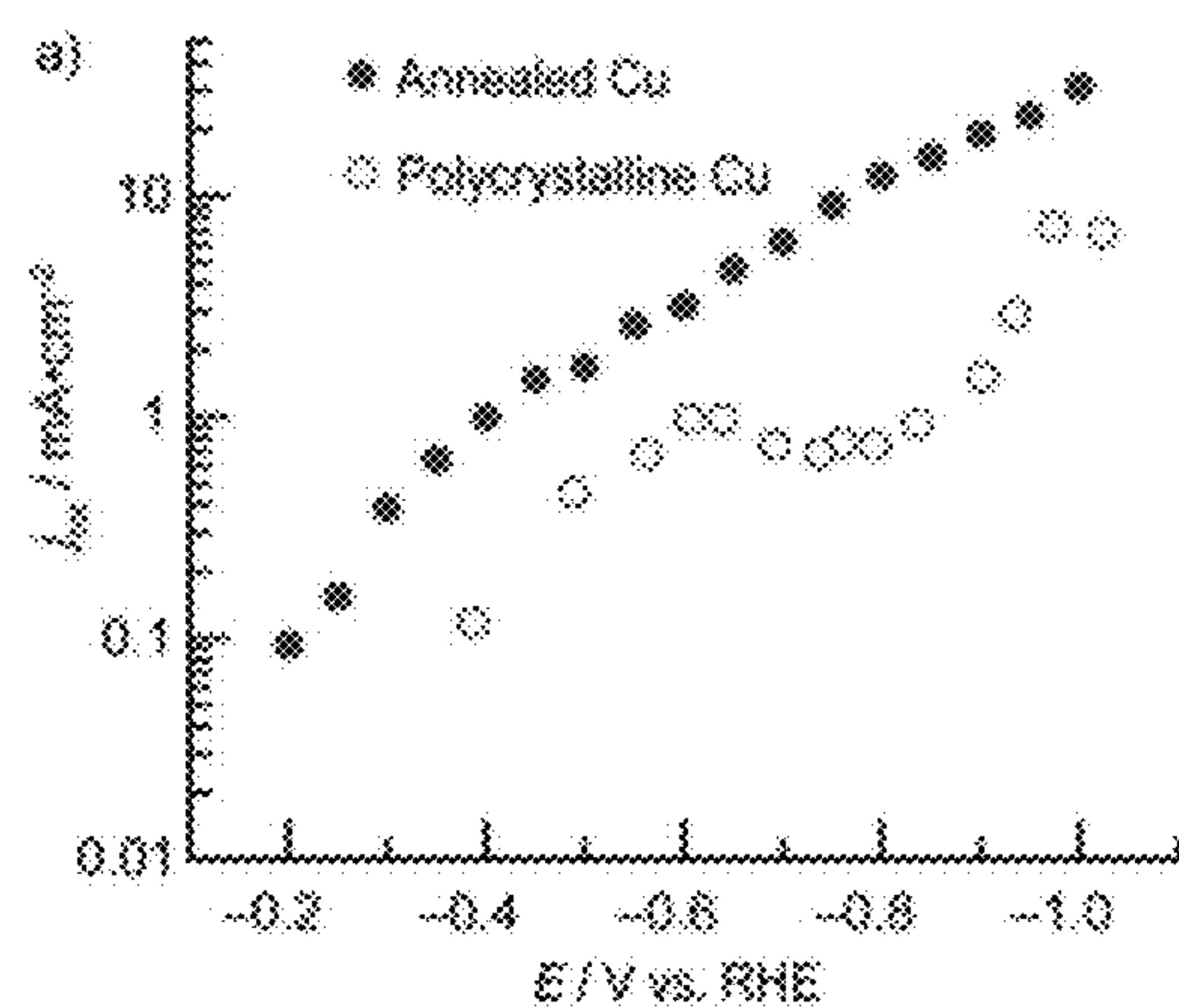


FIG. 6A

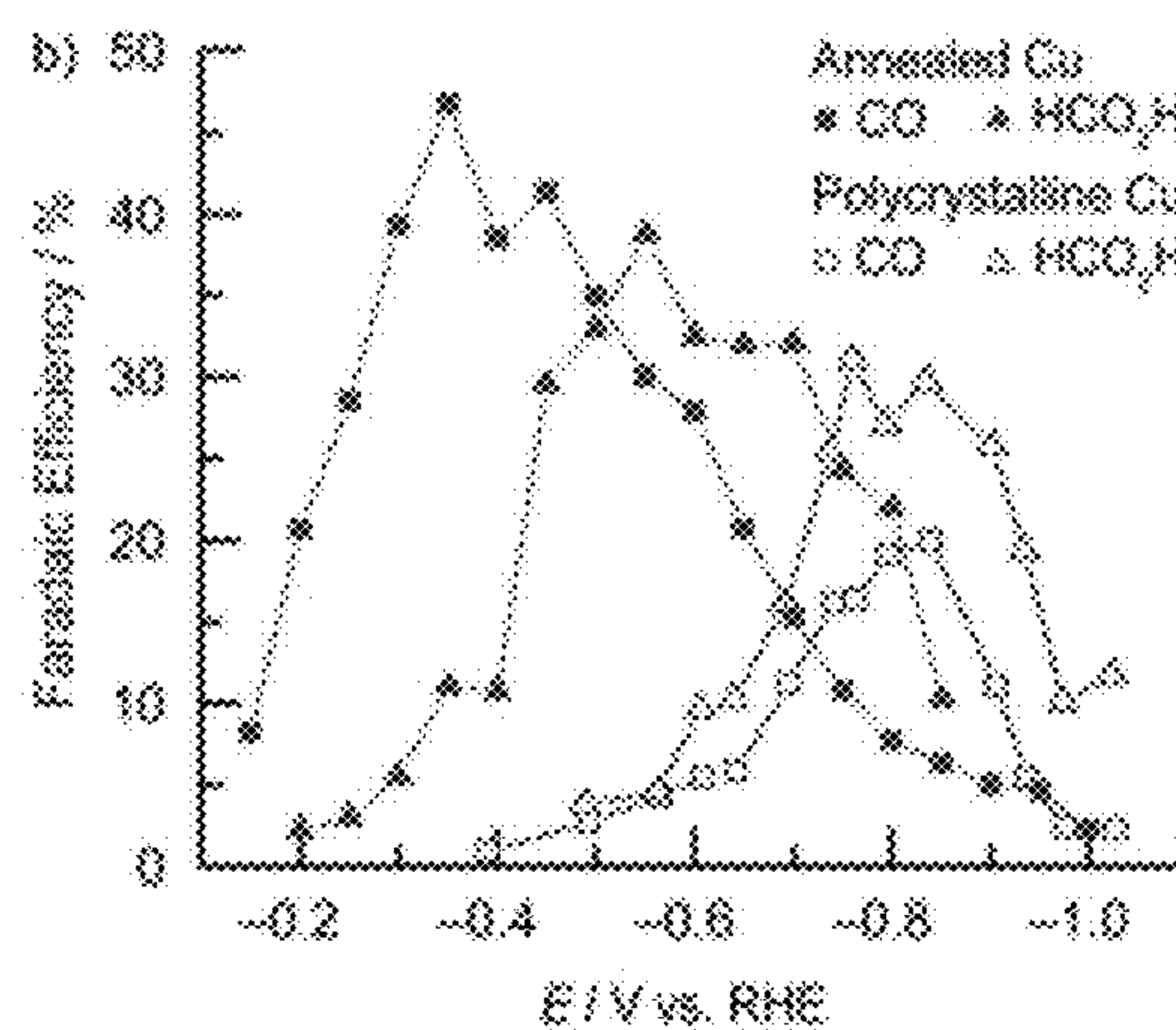


FIG. 6B

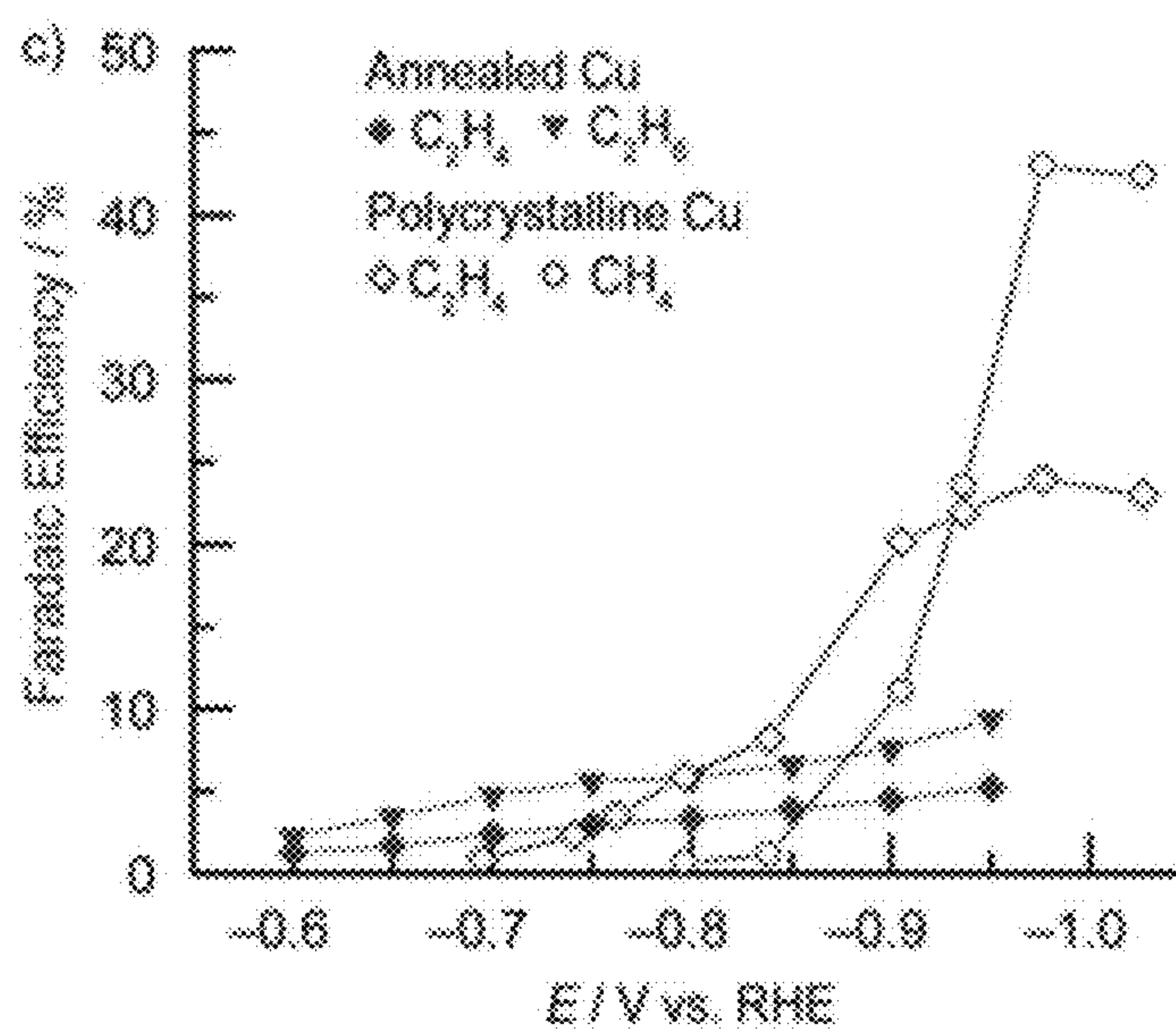


FIG. 6C

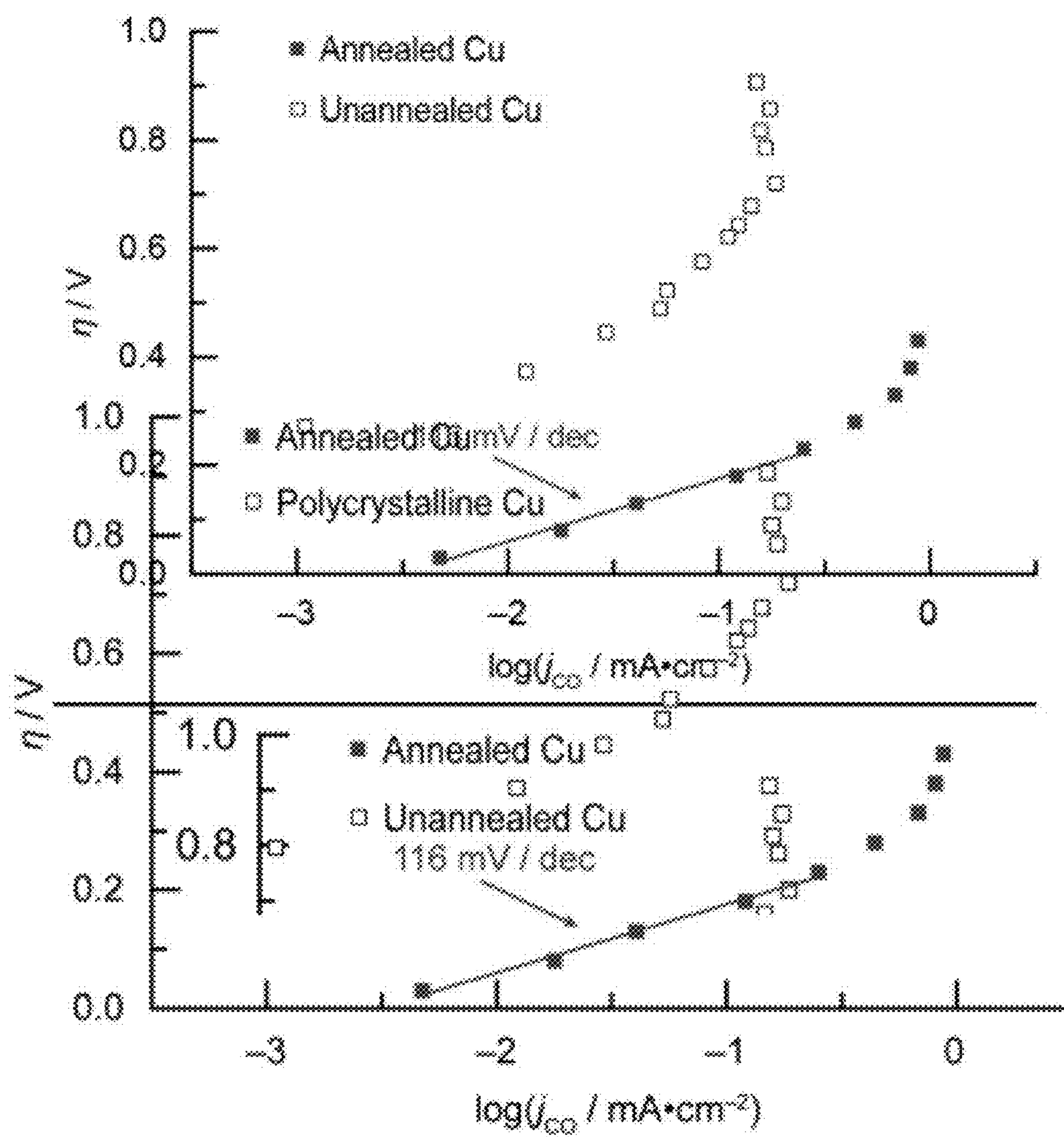


FIG. 7

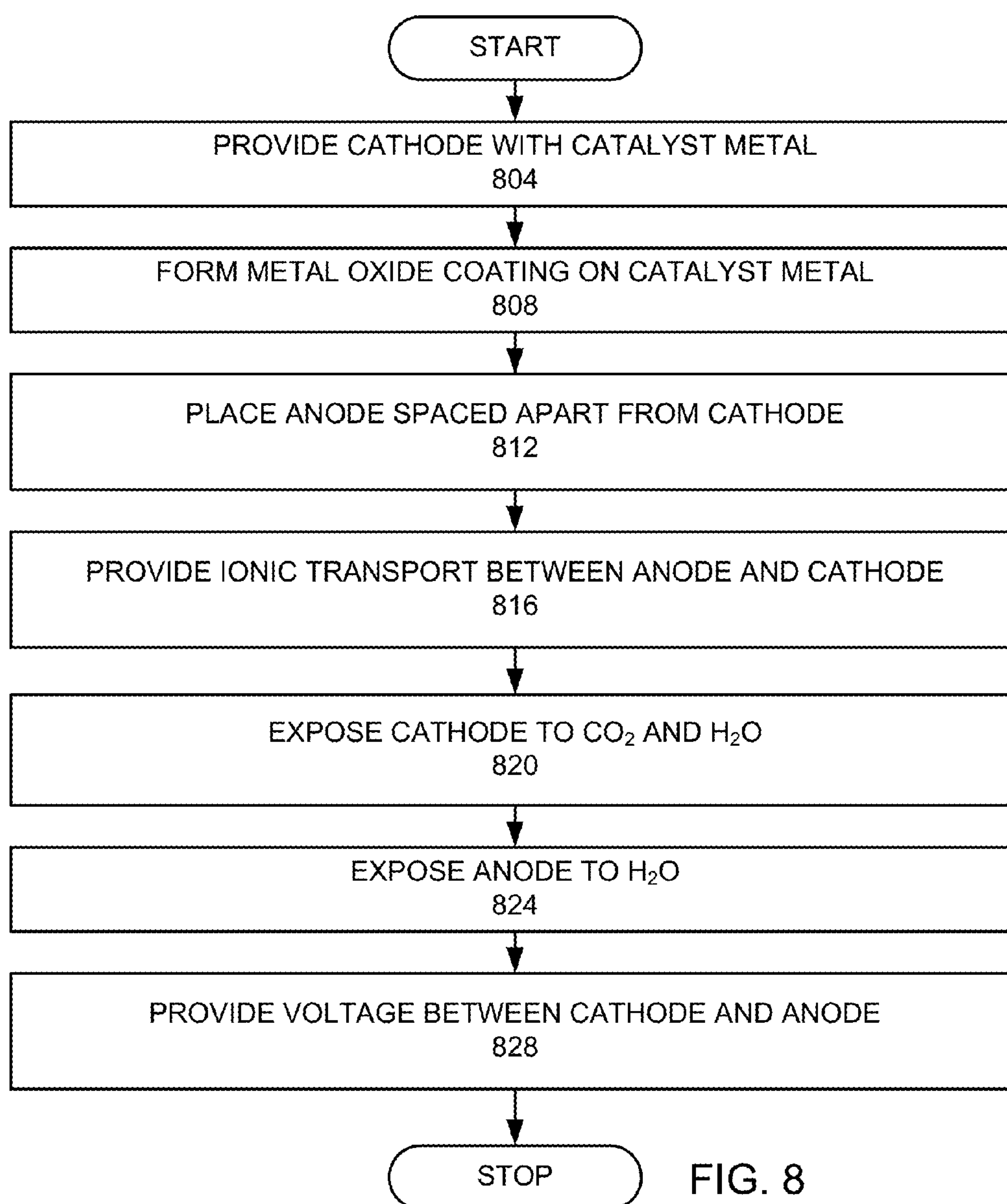


FIG. 8

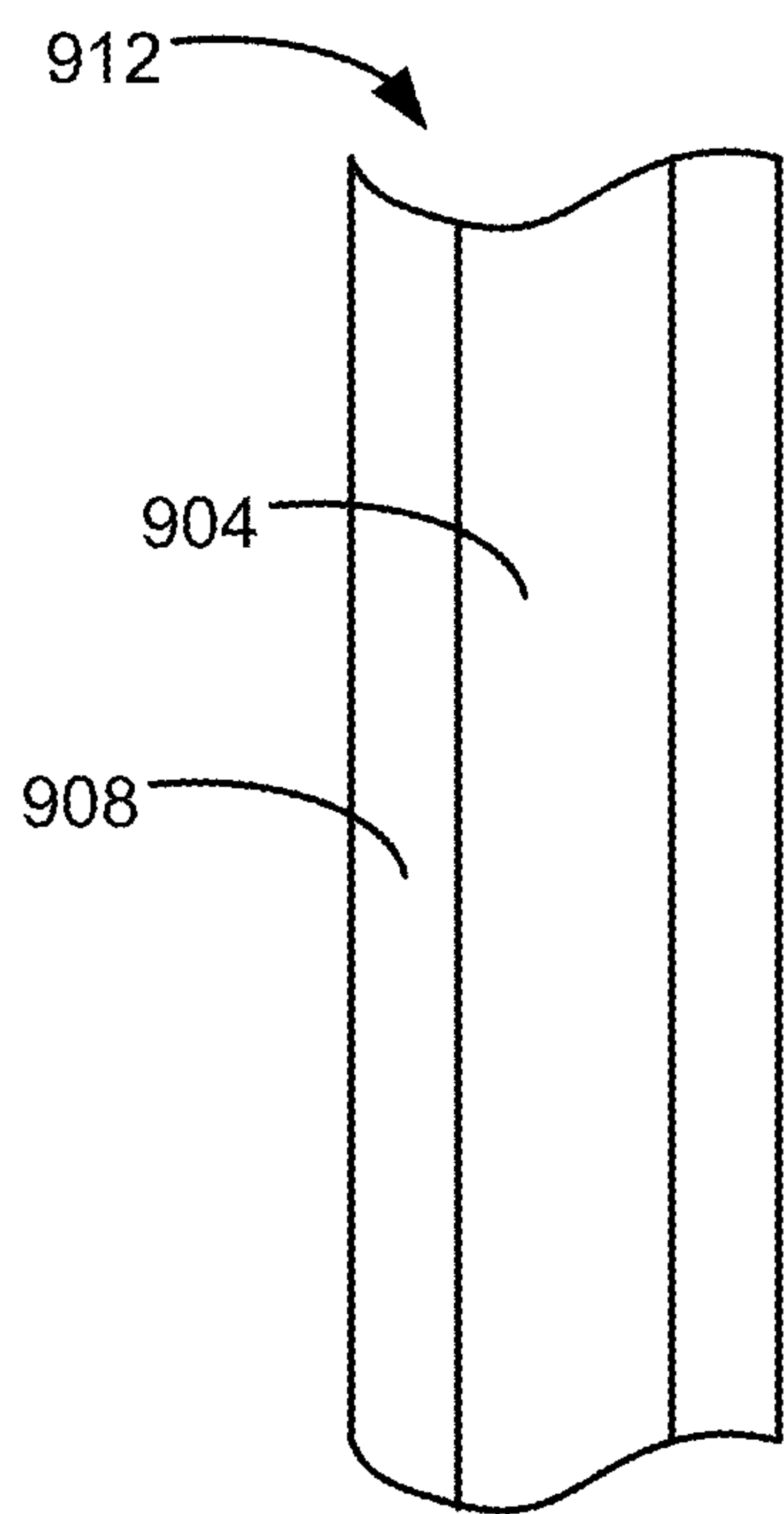


FIG. 9A

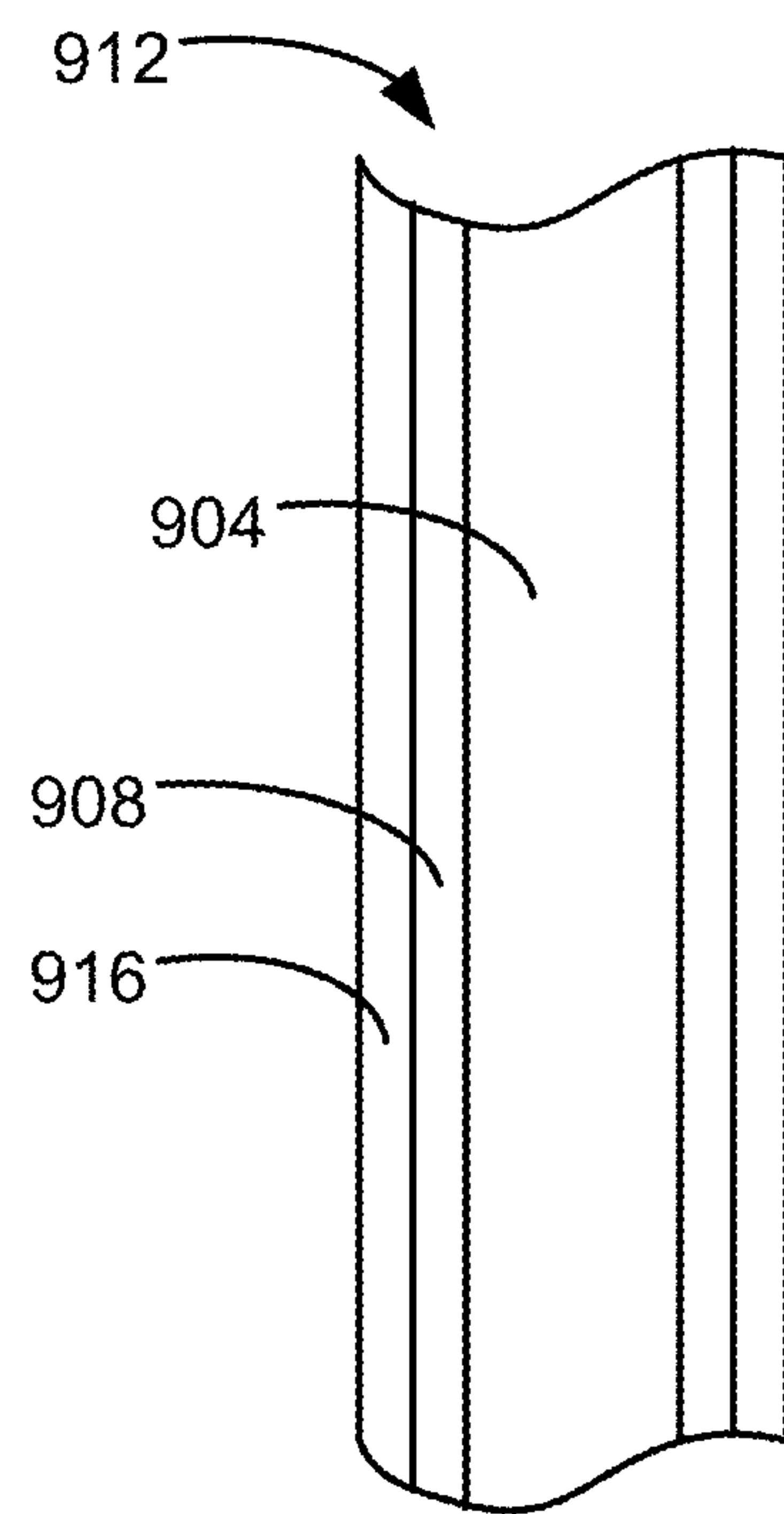


FIG. 9B

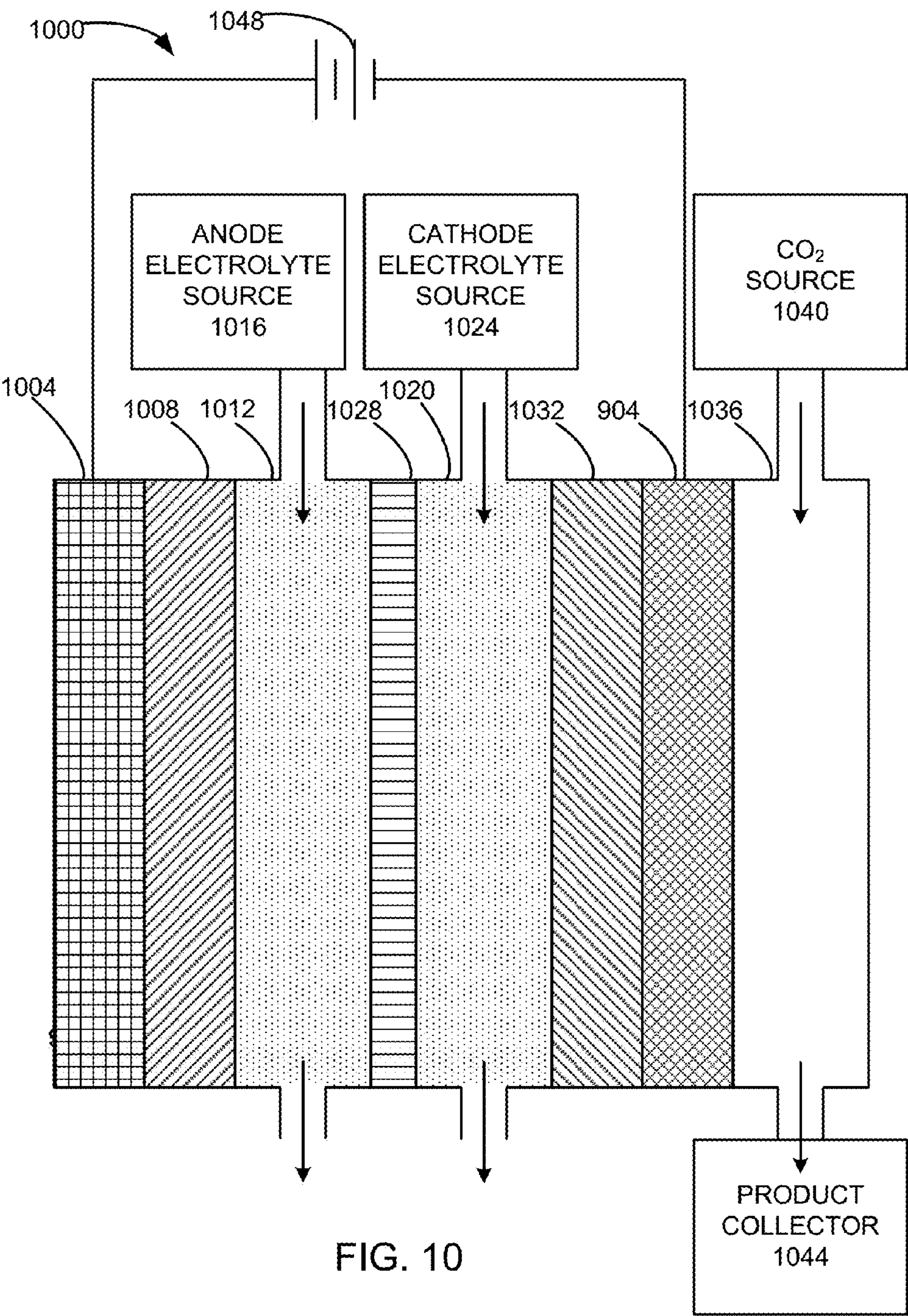
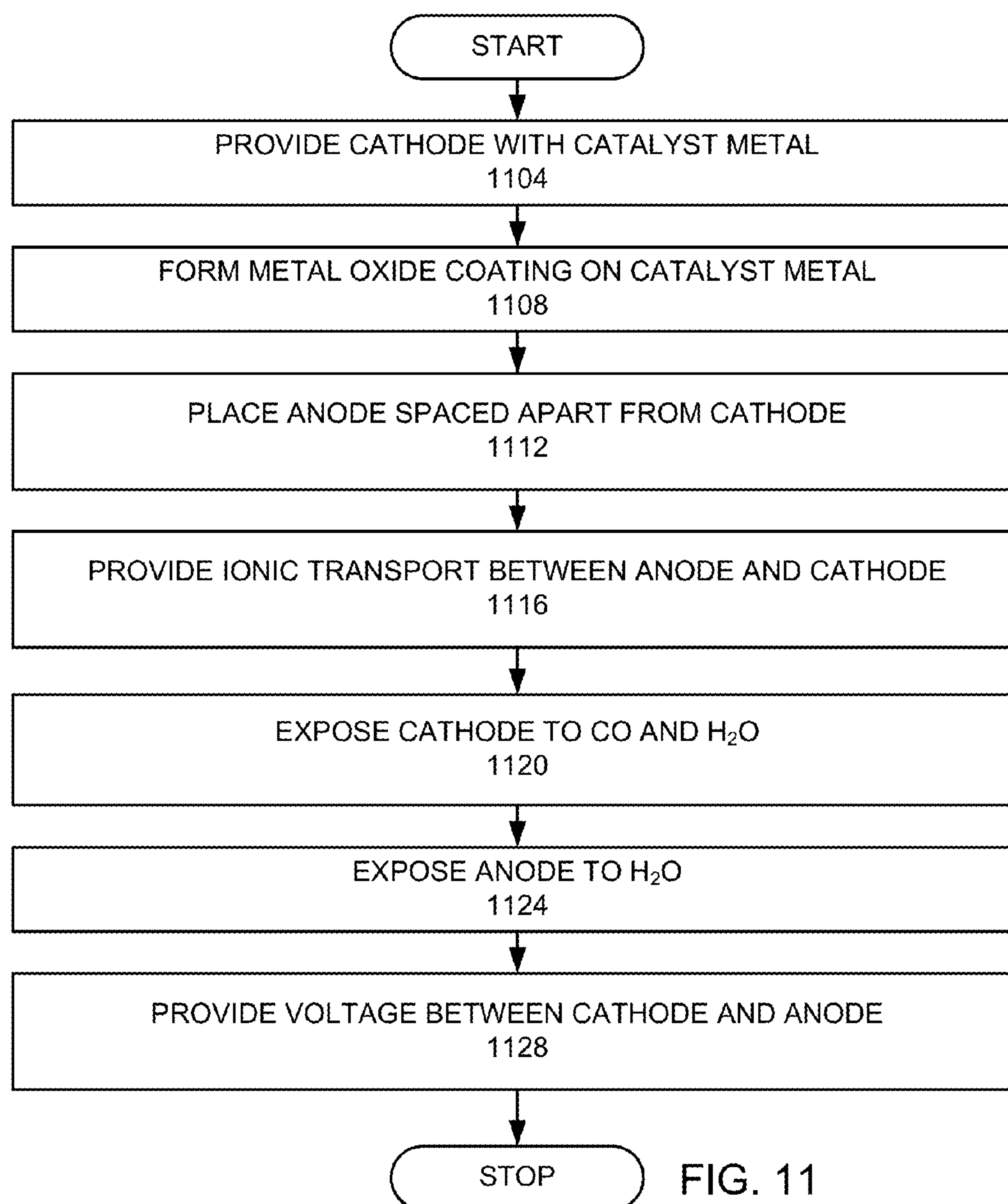
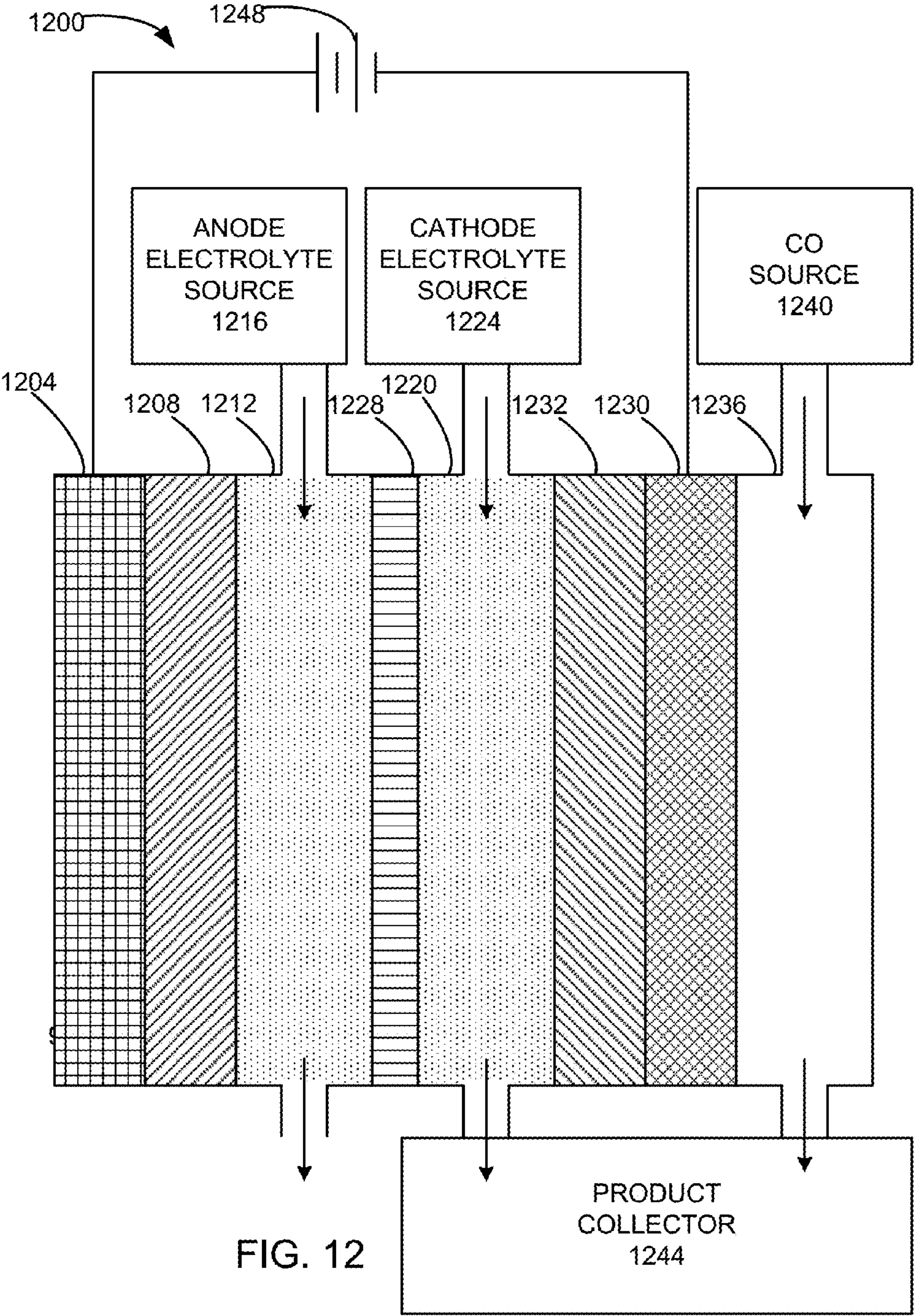


FIG. 10





CATALYSTS FOR LOW TEMPERATURE ELECTROLYTIC CO REDUCTION

CROSS REFERENCE TO RELATED APPLICATIONS

[0001] This application is a continuation of International Application No. PCT/US2013/025791 filed on Feb. 12, 2013, which is incorporated herein by reference for all purposes.

BACKGROUND OF THE INVENTION

[0002] This invention relates generally to the reduction of CO. Sustainable production of C-based fuel requires using renewable energy to power the reductive fixation of CO.

SUMMARY OF THE INVENTION

[0003] In accordance with the invention, a method for electrochemically reducing CO is provided. A cathode is provided, wherein the cathode comprises a conductive substrate with a catalyst of a metal and a metal oxide based coating on a side of the cathode. An anode is spaced apart from the cathode. An ionic transport is provided between the anode and cathode. The cathode is exposed to CO and H₂O. The anode is exposed to H₂O. A voltage is provided between the cathode and anode.

[0004] In another manifestation of the invention, a method for electrochemically reducing CO is provided. A coating is formed on a cathode by heating a metal layer of the cathode in air, electrochemically oxidizing the metal layer of the cathode, or by a metal oxide deposition to form a metal and metal oxide interface. An anode is spaced apart from the cathode. An ionic transport is provided between the anode and cathode. The coating is exposed to CO and H₂O. The anode is exposed to H₂O. A voltage is provided between the cathode and anode.

[0005] In another manifestation of the invention an apparatus, for electrochemically reducing CO is provided. An anode is provided. An oxidized cathode is spaced apart from the anode. A chamber for exposing the anode and oxidized cathode to at least one electrolyte is adjacent to the anode and oxidized cathode. A gas chamber for exposing the oxidized cathode to CO is adjacent to the oxidized cathode. A CO source for providing CO to the gas chamber is connected to the gas chamber.

[0006] The invention and objects and features thereof will be more readily apparent from the following detailed description and appended claims when taken with the drawings.

BRIEF DESCRIPTION OF THE DRAWINGS

[0007] FIG. 1A shows the XPS spectra of untreated Sn foil before and after electrolysis and Sn foil after etching in HBr.

[0008] FIG. 1B is a plot of total current density vs time, CO faradaic efficiency vs time, and overall HCO₂H faradaic efficiency at -0.7 V vs RHE in CO₂-saturated 0.5 M NaHCO₃ for unetched Sn.

[0009] FIG. 1C is a plot of total current density vs time, CO faradaic efficiency vs time, and overall HCO₂H faradaic efficiency for untreated Sn at -0.7 V vs RHE in CO₂-saturated 0.5 M NaHCO₃ for etched Sn.

[0010] FIG. 2A depicts the bulk electrolysis trace at -0.7 V in NaHCO₃/CO₂ electrolyte for a Ti cathode before and after the addition of 1 mM SnCl₂ to the electrolyte.

[0011] FIG. 2B shows SEM images of a Ti electrode before and after deposition showing the formation of a porous, particulate film with ~100 nm-diameter pieces atop a more uniform layer.

[0012] FIG. 2C is a high resolution Sn 3d_{5/2} XPS of a Sn/SnO_x catalyst removed 30 min or 12 h after the addition of Sn²⁺.

[0013] FIG. 2D provides graphs of XRD patterns showing Sn⁰, SnO₂, and Ti peaks after 30 min or 12 h.

[0014] FIGS. 3A-C shows the comparison of CO₂ reduction catalysis for unexcited Sn foil and in situ deposited Sn/SnO_x thin film electrodes.

[0015] FIGS. 4A-E shows the total geometric current density (*j_{tot}*) vs time, the faradaic efficiency (FE) for CO vs time and the overall FE for HCO₂H for the polycrystalline Cu electrode and several of the annealed electrodes with progressively thicker initial Cu₂O layers at -0.5 V vs the reversible hydrogen electrode.

[0016] FIG. 4F shows the average FE for CO vs the amount of charge required to reduce the Cu₂O layer per electrode area.

[0017] FIGS. 5A-F show the scanning electron microscopy (SEM) images, X-ray diffraction (XRD) patterns, and high-resolution Cu 2p X-ray photoelectron spectroscopy (XPS) spectra for a Cu electrode after annealing procedure and after subsequent CO₂ reduction electrolysis.

[0018] FIGS. 6A-C show the total current densities and faradaic efficiencies for the major products for a Cu electrode annealed at 500° C. for 12 h and for polycrystalline Cu.

[0019] FIG. 7 shows Tafel data for a Cu electrode annealed at 500° C. for 12 h and Tafel data for polycrystalline Cu.

[0020] FIG. 8 is a high level flow chart of an embodiment of the invention.

[0021] FIGS. 9A-B are enlarged cross-sectional views of part of a conductive substrate with a metal coating, forming part of a cathode.

[0022] FIG. 10 is a schematic view of an electrolyzer that may be used in an embodiment of the invention.

[0023] FIG. 11 is a high level flow chart of another embodiment of the invention.

[0024] FIG. 12 is a schematic view of an electrolyzer that may be used in another embodiment of the invention.

DETAILED DESCRIPTION OF ILLUSTRATED EMBODIMENTS

Tin

[0025] Metal electrodes have been the focus of extensive CO₂ electroreduction studies in aqueous solutions at ambient temperature. Sn has attracted considerable interest because it is one of the most active metals and its low cost is amenable to large-scale use. Despite its appeal relative to other electrodes, the energy efficiency of Sn is too low for practical electrolysis. Sn is reported to require at least 0.86 V of overpotential to attain a CO₂ reduction partial current density of 4-5 mA/cm² in an aqueous solution saturated with 1 atm of CO₂. It is generally assumed that the bare Sn surface is the catalytically active surface for CO₂ reduction. The large overpotential required for CO₂ reduction is thought to result from the barrier associated with the initial e⁻ transfer to form a CO₂^{•-} intermediate that is poorly stabilized by the Sn surface. This mechanistic scenario is commonly invoked for many metal electrodes.

[0026] In an embodiment of the invention, SnO_x is essential to CO_2 reduction catalysis on Sn. This may be shown by demonstrating that removal of SnO_x from a Sn electrode results in nearly exclusive H_2 evolution activity. This insight is subsequently applied to prepare a composite Sn/ SnO_x thin film catalyst that exhibits greatly enhanced CO_2 reduction activity relative to a typical Sn electrode.

[0027] To evaluate the importance of SnO_x on the surface of Sn in CO_2 reduction, we compared the activity of Sn electrodes that had been etched in strong acid to the activity of untreated electrodes. In both cases, new pieces of high purity Sn foil (99.998%) were used. The surface of the untreated foil was examined by XPS to characterize the native SnO_x layer. FIG. 1A shows the XPS spectra of untreated Sn foil before and after electrolysis (left) and Sn foil after etching in HBr (right). The curves are combinations of two Gaussian/Lorentzian curves at 486.5 eV and 484.7 eV. FIG. 1B is a plot of total current density vs time (indicated by the line), CO faradaic efficiency vs time (indicated by the ■ points) and overall HCO_2H faradaic efficiency for untreated Sn at -0.7 V vs RHE in CO_2 -saturated 0.5 M NaHCO_3 for unetched Sn. FIG. 1C is a plot of total current density vs time (indicated by the line), CO faradaic efficiency vs time (indicated by the ■ points) and overall HCO_2H faradaic efficiency for untreated Sn at -0.7 V vs RHE in CO_2 -saturated 0.5 M NaHCO_3 for etched Sn.

[0028] The high resolution Sn $3d_{5/2}$ spectrum was fit to two peaks at 486.5 eV and 484.7 eV that correspond to $\text{Sn}^{4+/2+}$ (SnO_x) and Sn^0 , respectively. The ratio of corrected peak areas for SnO_x to Sn^0 is 95:5, indicating the presence of a >5 nm native SnO_x layer.

[0029] Etched electrodes were prepared by immersing the Sn foil in 24% HBr at 90°C . for 10 min. An XPS spectrum of the etched electrode taken immediately after removal from the HBr solution exhibited a $\text{SnO}_x:\text{Sn}^0$ ratio of 17:83 (FIG. 1A). The residual oxide observed on this electrode is likely due to oxide regrowth in the brief exposure to air upon transferring to the XPS chamber, as assessed by independent XPS experiments with a sputtered electrode. For electrolysis experiments, etched electrodes were rinsed with deionized water at the conclusion of the etching procedure and used immediately to minimize oxide regrowth.

[0030] The electrolyses were performed in an H-cell in 0.5 M aqueous NaHCO_3 saturated with CO_2 (" $\text{NaHCO}_3/\text{CO}_2$ ") at a potential of -0.7 V vs the reversible hydrogen electrode (RHE; all potentials are referenced to this electrode). The headspace of the cathodic compartment was continuously purged with CO_2 into the sampling valve of a gas chromatograph (GC), enabling periodic quantification of the gas phase products. FIG. 1B shows the total geometric current density (j_{tot}) vs time and the faradaic efficiency for CO production at various time points for an untreated Sn electrode. The electrode exhibits a current density of 0.4-0.6 mA/cm^2 and a steady-state faradaic efficiency for CO of 5-10%. NMR analysis of the electrolyte at the conclusion of the experiment indicates 19% faradaic efficiency for HCO_2H ; the remainder of the current is accounted for by H_2 formation. This CO_2 reduction activity is consistent with the best reported activity for Sn at -1.06 V, taking into account the difference in overpotential. An electrode examined by XPS after a 12 h electrolysis at -0.7 V exhibited a $\text{SnO}_x:\text{Sn}^0$ ratio of 89:11, indicating that the native SnO_x layer is stable to the reduction conditions (FIG. 1A).

[0031] Strikingly, an etched Sn electrode exhibits a much higher j_{tot} of 3-4 mA/cm^2 , but very low faradaic efficiency for

CO (0.5%) and HCO_2H production (0.3%) (FIG. 1C). The higher j_{tot} likely reflects a larger electrochemical surface area due to etching. Despite the higher surface area, the geometric partial current density for CO_2 reduction is lower for the etched Sn electrode (24-32 $\mu\text{A}/\text{cm}^2$) than the untreated Sn electrode (92-140 $\mu\text{A}/\text{cm}^2$) due to the much lower faradaic efficiency. Very low ($<1\%$) CO_2 reduction faradaic efficiencies on etched Sn are also observed over a range of potentials from -0.5 V to -1.0 V. Thus, etched Sn is a moderately efficient H_2 evolution catalyst, but is essentially inactive for CO_2 electroreduction. Similar results were obtained if Sn electrodes were etched by polarizing at -3 V in HCl solution instead of treating with hot HBr solution.

[0032] Together, the XPS and electrolysis results indicate that removal of the native SnO_x layer from a Sn electrode suppresses CO_2 reduction activity such that H_2 evolution accounts for $>99\%$ of the current density. The small residual CO_2 reduction activity observed on etched Sn likely reflects the growth of a small amount of SnO_x on the etched electrode before the start of electrolysis.

[0033] Based on these results, we hypothesized that the simultaneous deposition of Sn^0 and SnO_x on an electrode surface would result in a material with enhanced Sn— SnO_x contact that is consequently a more active catalyst for CO_2 reduction than a typical Sn foil electrode with a native SnO_x layer. Accordingly, we sought electrodeposition conditions in which the hydrolysis of Sn^{2+} by cathodically generated OH^- would take place concurrently with the reduction of Sn^{2+} to Sn^0 ($E^0 = -0.1375$ V vs NHE). As described below, deposition on Ti electrodes under the same conditions used for CO_2 electroreduction proved to be particularly effective.

[0034] FIG. 2A depicts the bulk electrolysis trace at -0.7 V in $\text{NaHCO}_3/\text{CO}_2$ electrolyte for a Ti cathode before and after the addition of 1 mM SnCl_2 to the electrolyte. Prior to the addition of Sn^{2+} , the Ti electrode exhibits a current density of $-10 \mu\text{A}/\text{cm}^2$ with very little detectable CO_2 reduction. Addition of Sn^{2+} results in a sharp rise in the current density to a steady-state value of $\sim 1.8 \text{ mA}/\text{cm}^2$ and the formation of a grey deposit on the electrode surface. The current density is stable for >10 h and corresponds to $>85\%$ CO_2 reduction with the remainder accounted for by H_2 evolution. Nearly identical results are obtained if $\text{Sn}(\text{OTf})_2$ is used instead of SnCl_2 , indicating that Cl^- is not necessary for catalyst formation.

[0035] The composition and structure of the electrodeposited catalyst were characterized by a combination of scanning electron microscopy (SEM), XPS and powder x-ray diffraction (XRD). A catalyst was prepared via in situ deposition as described above and removed from the electrolyte 30 min after the addition of Sn^{2+} . FIG. 2B shows SEM images of a Ti electrode before (left) and after (right) deposition showing the formation of a porous, particulate film with ~ 100 nm-diameter pieces atop a more uniform layer. FIG. 2C is a high resolution Sn $3d_{5/2}$ XPS of a Sn/ SnO_x catalyst removed 30 min (left) or 12 h (right) after the addition of Sn^{2+} . XPS analysis indicates a $\text{SnO}_x:\text{Sn}^0$ ratio of 93:7, similar to the ratio observed for Sn foil electrodes with a native SnO_x layer. FIG. 2D provides graphs of XRD patterns showing Sn^0 (■), SnO_2 (★) and Ti (●) peaks after 30 min or 12 h. In the XRD pattern of this electrode, strong Sn^0 peaks are observed along with small peaks that correspond to SnO_2 . The latter are absent for a Sn foil electrode with a native SnO_x . For comparison, a separate catalyst film was prepared and removed for analysis 12 h after the addition of Sn^{2+} . The XPS spectrum, shown in FIG. 2C, and XRD pattern for this electrode are very similar

to those of the sample removed after 30 min. Together, these results indicate that a composite Sn/SnO_x material is formed under the deposition conditions.

[0036] The electrodeposited catalyst (hereafter referred to as “Sn/SnO_x”) exhibits greatly enhanced CO₂ reduction catalysis compared to a typical Sn foil electrode with a native SnO_x layer. For both electrodes, CO, HCO₂H and H₂ together account for >99% of the reduction products in NaHCO₃/CO₂ electrolyte. To compare the activities of Sn foil and Sn/SnO_x, we measured their partial current densities for CO and HCO₂H at selected potentials between −0.5 and −0.7 V. Comparison of CO₂ reduction catalysis for Sn foil and in situ deposited Sn/SnO_x thin film electrodes are illustrated in FIGS. 3A-C. FIG. 3A shows Tafel plots for HCO₂H production. FIG. 3B shows Tafel plots for CO production. FIG. 3C is a bar graph showing Faradaic efficiencies for HCO₂H and CO at various potentials. These data were obtained by performing stepped-potential electrolyses with periodic quantification of the gaseous products by GC and removal of aliquots after each step for NMR analysis.

[0037] For Sn foil, approximate Tafel slopes of 74 mV/dec and 72 mV/dec are observed for HCO₂H and CO production, respectively. Similar Tafel slopes are observed for HCO₂H (67 mV/dec) and CO (77 mV/dec) production on Sn/SnO_x, however the geometric partial current densities are 7-8-fold higher than for Sn foil. The higher geometric current densities on Sn/SnO_x are not simply the result of greater electroactive surface area, as indicated by cyclic voltammetry and the dramatic differences in faradaic efficiencies for Sn foil and Sn/SnO_x. Over the range of potentials used for Tafel analysis, the CO faradaic efficiencies are 4-fold higher and the HCO₂H faradaic efficiencies are 2-3-fold higher on Sn/SnO_x than on untreated Sn foil.

[0038] The Tafel slopes for HCO₂H and CO production on both Sn foil and Sn/SnO_x are inconsistent with CO₂ reduction mechanisms that proceed through an initial rate-determining 1 e[−] transfer to CO₂. Such a mechanism would result in a 118 mV/dec slope. The observed slopes are instead much closer to 59 mV/dec, which supports mechanisms in which there is a reversible 1 e[−] transfer to CO₂ to form CO₂^{•−} prior to a chemical rate-determining step. Possibilities for the chemical rate-determining step include protonation of CO₂^{•−} or migration to an alternative site on the electrode surface. Competing rate-determining steps, such as protonation at C vs O of CO₂^{•−}, may determine the HCO₂H vs CO selectivity.

[0039] The Tafel data, combined with the absence of appreciable CO₂ reduction activity on etched Sn, suggest that SnO_x enables CO₂ reduction to occur by stabilizing CO₂^{•−}. At present, we cannot determine whether reduction takes place at the interface between Sn⁰ and SnO_x or on the SnO_x surface directly. In the absence of SnO_x to stabilize CO₂^{•−}, Sn⁰ only catalyzes H₂ evolution because the 1 e[−] transfer to CO₂ is prohibitively slow. The higher CO₂ reduction partial current density and faradaic efficiency on Sn/SnO_x relative to Sn foil with a native SnO_x layer are therefore indicative of a greater density of active sites for CO₂ reduction and a higher ratio of these sites to H₂ evolution sites for the in situ deposited catalyst.

[0040] The CO₂ reduction activity of Sn/SnO_x as indicated by the Tafel plots and faradaic efficiencies in FIGS. 3A-C, compares favorably to all polycrystalline metal electrodes in aqueous electrolytes with the exception of Au, which is comparably active initially, but subject to rapid deactivation. Improving CO₂ and ion mass transport by incorporating

Sn/SnO_x in a flow cell and/or a gas diffusion electrode may enable increasing the current density by 1-2 orders of magnitude without large overpotential increases. Elucidating the detailed mechanistic role of SnO_x in mediating electron transfer to CO₂ is an important objective toward this goal. Moreover, the importance of SnO_x to CO₂ reduction on Sn surfaces raises the possibilities that metal oxides may be involved in CO₂ reduction pathways on other metal electrodes and that the preparation of alternative metal/metal oxide composites may yield additional CO₂ reduction catalysts with superior activity.

Copper

[0041] Polycrystalline Cu has been the focus of most CO₂ reduction studies because it is one of the best available catalysts and is capable of producing hydrocarbon products. Although mechanistic studies have yielded valuable insights into the CO₂ reduction pathways on Cu, the principal shortcomings of this electrode have not been addressed. Most significantly, the energetic efficiency of Cu is limited by the large overpotential (>0.7 V) required for CO₂ reduction to outcompete H₂O reduction. In addition, Cu electrodes rapidly lose their CO₂ reduction activity unless stringently purified electrolytes are used, a requirement that is not compatible with scalable fuel synthesis.

[0042] Achieving efficient Cu-catalyzed CO₂ reduction requires preparing Cu particles whose surfaces have active sites that are different from those on the surface of a polycrystalline Cu electrode. Electrochemical reduction of metal oxides provides one possible route to metal particles with altered surface structures. Researchers have previously used electrochemical methods including potential cycling and anodic pulses to form and subsequently reduce oxides on Cu electrodes. These treatments have resulted in increased hydrogen evolution activity in alkaline electrolytes and altered product selectivity at high overpotential in CO₂ reduction electrolyses. While these studies provide evidence of altered electrocatalytic properties, substantial improvements to the energetic efficiency of CO₂ reduction have not been observed. Researchers have also used copper oxide electrodes in CO₂ reduction electrolyses. The oxides were reduced to Cu⁰ in situ during CO₂ reduction catalysis, but only transient changes in the CO₂ product distribution attributed to oxide catalysis were observed. Here we show that the CO₂ reduction properties of Cu⁰ electrodes resulting from copper oxide reduction vary widely depending on the properties of the initial oxide layer. Reduction of thick Cu₂O layers formed by high temperature annealing results in electrodes that catalyze energy-efficient CO₂ reduction and are stable to the deactivation phenomena that plague bulk metal electrodes.

[0043] Electrodes were prepared by electropolishing pieces of polycrystalline Cu foil (99.9999%) in 85% phosphoric acid and subsequently annealing the electrodes in air at selected temperatures for variable amounts of time. The activities of these electrodes were compared to that of a polycrystalline Cu electrode in controlled potential electrolyses performed in CO₂-saturated 0.5 M NaHCO₃ electrolyte (“NaHCO₃/CO₂”) in a two-compartment electrolysis cell. The headspace of the cathodic chamber was continuously purged with CO₂ into the sampling loop of a gas chromatograph (GC) to enable periodic quantification of the gas-phase

products. The solution-phase products were quantified by NMR analysis of the electrolyte at the conclusion of the electrolyses.

[0044] FIGS. 4A-E shows the total geometric current density (j_{tot}) vs time, the faradaic efficiency (FE) for CO vs time and the overall FE for HCO₂H for the polycrystalline Cu electrode (FIG. 4A) and several of the annealed electrodes (FIG. 4B-E) with progressively thicker initial Cu₂O layers at -0.5 V vs the reversible hydrogen electrode (RHE; all potentials are referenced to this electrode). The polycrystalline Cu electrode exhibited a j_{tot} of ~100 μ A/cm², a FE for CO that declined from 10% at the start of the electrolysis to <2% over the course of 7 h and a FE for HCO₂H of 3%. The majority of the current, >90%, was due to H₂ evolution. These values are consistent with the previously measured activity for Cu in KHCO₃ electrolytes. Annealing Cu at 130° C., the temperature used to prepare Cu₂O electrodes for most previous studies, had very little effect on the activity under these conditions. The electrode annealed at 130° C. for 12 h (FIG. 4B) exhibited a j_{tot} of 10 mA/cm² during the first 4 s in which the thin Cu₂O layer was reduced. Subsequently, the j_{tot} and FEs were very similar to those of the polycrystalline electrode.

[0045] In contrast to these results, the electrodes annealed at higher temperatures exhibited larger j_{tot} values and improved CO₂ reduction FEs upon reduction of the Cu₂O layer. The electrode annealed at 300° C. for 30 min exhibited an initial j_{tot} of 10 mA/cm² for 2 min as the Cu₂O was reduced and subsequently a stable j_{tot} of 1.0 mA/cm². The FE for CO was 25% during the first hour of electrolysis before declining to 10% over 7 h; the FE for HCO₂H on the reduced electrode was 5%. Further improvements were obtained by starting with a thicker Cu₂O layer. After Cu₂O reduction of the electrode annealed at 300° C. for 5 h, j_{tot} reached a stable value of 1.3 mA/cm², the FE for CO reached 35% and the FE for HCO₂H was 24% (FIG. 4D). Annealing at 500° C. for 12 h resulted in an even thicker Cu₂O layer and a stable j_{tot} of 2.7 mA/cm². This electrode produced CO with ~40% FE and HCO₂H with 33% FE. Notably, the FE for CO was maintained at 40% throughout the electrolysis, indicating not only efficient but also stable activity for CO₂ reduction on this surface.

[0046] A plot of the average CO FEs for the annealed electrodes vs the amount of charge passed per electrode area (Q) in the Cu₂O reduction is shown in FIG. 4F. The FEs increased with the amount of charge passed until reaching a plateau at 30-40% for $Q \geq 5$ C/cm². Assuming bulk density of Cu₂O on the electrode, 5 C/cm² corresponds to a ~3 μ m-thick layer. Together, these results demonstrate that a threshold thickness of the initial Cu₂O layer is required to achieve both efficient and stable CO₂ reduction catalysis for the electrode resulting from Cu₂O reduction.

[0047] Based on these results, electrodes prepared by annealing Cu at 500° C. for 12 h were selected for further characterization and CO₂ reduction studies. FIGS. 5A-F show the scanning electron microscopy (SEM) images (FIGS. 5A, D), X-ray diffraction (XRD) patterns (FIGS. 5B, E), and high-resolution Cu 2p X-ray photoelectron spectroscopy (XPS) spectra (FIGS. 5C, F) for a Cu electrode after this annealing procedure (FIGS. 5A-C) and after subsequent CO₂ reduction electrolysis (FIGS. 5D-F). After annealing, the SEM showed a dense array of rods with 100-1000 nm diameters on the electrode surface. These rods are the outermost portion of a thick Cu₂O layer coating the electrode, as evidenced by the large Cu₂O peaks and the near complete sup-

pression of the Cu⁰ peaks in the XRD pattern. The characteristic Cu²⁺ satellite peaks in the XPS spectrum are consistent with the presence of a thin (<10 nm) CuO layer coating the Cu₂O. Following CO₂ reduction electrolysis, SEM indicated that the rod morphology was intact, but smaller particles (~20 nm) were embedded within the rods (FIG. 5D and Figure S3). Only Cu⁰ peaks were observed in the XRD pattern, FIG. 5F. The Cu 2p XPS spectrum indicated the presence of Cu⁰ or Cu¹⁺ but the peaks associated with Cu²⁺ in the spectra prior to electrolysis were absent. Together, these results indicate the complete reduction of the Cu₂O layer, although we cannot rule out the presence of a thin, metastable Cu₂O layer or other surface-bound Cu¹⁺ species during electrocatalysis.

[0048] The electrochemically active surface area of a reduced electrode that had been annealed at 500° C. for 12 h was determined by measuring the double layer capacitance in 0.1 M HClO₄ after CO₂ reduction electrolysis. The capacitance was 13.9 mF/cm², which is 475× larger than the capacitance of 29 μ F/cm² measured for a polycrystalline Cu electrode. This roughness factor is considerably larger than the difference in j_{tot} between the two electrodes (~30×), consistent with the difference in FEs between the two electrodes.

[0049] The presence of 100-1000 nm rods observed in FIG. 5D is not necessary for efficient CO₂ reduction. Electrodes annealed at temperatures $\geq 500^\circ$ C. for variable amounts of time exhibited very different morphological features on this length scale, but nonetheless comparable FEs for CO₂ reduction at -0.5 V. These results suggest that the CO₂ reduction efficiency of electrodes annealed at high temperatures is associated with a Cu particle surface or grain boundary structure that forms when suitably thick Cu₂O layers are electrochemically reduced.

[0050] To further characterize the effect of high temperature annealing on the CO₂ reduction activity of Cu, we measured the partial current densities for the reduction products at a variety of potentials between -0.2 V and -1.0 V in NaHCO₃/CO₂ using an electrode that had been annealed at 500° C. for 12 h (hereafter referred to as “annealed Cu”). The total current densities and faradaic efficiencies for the major products are shown in FIGS. 6A-C, which provides comparisons of electrocatalytic activities of polycrystalline Cu and Cu annealed at 500° C. for 12 h. FIG. 6A is a graph of total current density vs. potential. FIG. 6B is a graph of faradaic efficiencies for CO and HCO₂H vs potential. FIG. 6C is a graph of faradaic efficiencies for CH₄, C₂H₄ and C₂H₆ vs potential. Attempts to collect the corresponding data under identical conditions with polycrystalline Cu were unsuccessful due to the rapid degradation of catalytic activity. Instead, optimal data from previous studies with polycrystalline Cu at several potentials in 0.1 M KHCO₃ are included for comparison.

[0051] The annealed Cu electrode exhibits a high efficiency for CO₂ reduction at remarkably low overpotentials. A peak faradaic efficiency of ~45% for CO production is obtained at potentials ranging from -0.3 V to -0.5 V, corresponding to 0.19 V to 0.39 V of overpotential for this product (FIG. 6B). By comparison, essentially no CO₂ reduction to CO is observed for polycrystalline Cu in this potential range; the maximum efficiency for CO with polycrystalline Cu is 20%, which requires -0.8 V ($\eta=0.69$ V). Similarly, annealed Cu attains a peak faradaic efficiency for HCO₂H production of 30% at potentials ranging from -0.45 V to -0.65 V ($\eta=0.25$ V

to 0.45 V), whereas polycrystalline Cu requires -0.7 V to -0.9 V ($\eta=0.5$ V to 0.7 V) to attain a comparable faradaic efficiency (FIG. 6B).

[0052] At relatively negative potentials (<-0.6 V), annealed Cu catalyzes the reduction of CO_2 to ethylene and ethane (FIG. 6C). In contrast, polycrystalline Cu produces only ethylene and methane at high overpotential. Previous work on Cu single crystals has shown that the ratio of ethylene to methane can be boosted by introducing (111) steps in the (100) basal plane, i.e. by using single crystal Cu electrodes with a high index face exposed to the solution. However, methane was never fully suppressed and no ethane was observed in these studies. These results indicate that the surface structures of the Cu particles produced by Cu_2O reduction are distinct from the structures of the high index faces of Cu. We also note that no methanol was detected among the reduction products for annealed Cu at any potential examined here, in contrast to what has been reported for CO_2 reduction catalysis with Cu electrodes annealed at lower temperatures.

[0053] The faradaic efficiencies for the hydrocarbon products on annealed Cu are low and H_2 is the major product at high overpotentials. This difference relative to the lower overpotential regime most likely reflects the mass transport limitations at the high current densities observed (>10 mA/cm²) rather than the intrinsic selectivity of the electrode. Improvements in mass transport by using a flow cell or gas diffusion electrode are expected to enable substantially higher CO_2 reduction current densities without large overpotential increases.

[0054] To obtain insight into the mechanistic pathway(s) for CO_2 reduction with annealed Cu, a plot of overpotential vs the log of the partial current density for CO production (a Tafel plot) was extracted from the data described above. The data are shown in FIG. 7 along with Tafel data for polycrystalline Cu. The plot for annealed Cu is linear over the range of overpotentials from 0.05 V to 0.3 V with a slope of 116 mV/decade. This slope is consistent with a rate-determining initial electron transfer to CO_2 to form a surface-adsorbed $\text{CO}_2^{\bullet-}$ intermediate, a mechanism that is commonly invoked for metal electrodes. A similar slope is evident in the plot for polycrystalline Cu. The dramatic difference in FE between the two electrodes suggests that the Cu surfaces formed by reducing thick Cu_2O layers enable formation of the $\text{CO}_2^{\bullet-}$ intermediate while suppressing H_2O reduction.

[0055] In summary, our results show that Cu particles prepared by reducing μm -thick Cu_2O films catalyze the reduction of CO_2 to CO and HCO_2H with high faradaic efficiencies at exceptionally low overpotentials and produce C2 hydrocarbons to the exclusion of CH_4 at high overpotentials. Electrodes with these characteristics can readily be prepared with high surface areas, enabling >1 mA/cm² geometric current densities for CO_2 reduction at <0.4 V overpotential and measurable CO_2 reduction current densities at <0.1 V overpotential, levels of activity that were previously inaccessible with metal electrodes under comparable conditions. Furthermore, CO_2 reduction with these electrodes is resistant to deactivation for at least several hours, a marked improvement over the rapid deactivation of polycrystalline Cu under identical conditions. We anticipate that elucidation of the surface structures of the Cu particles formed by reducing thick Cu_2O layers will provide crucial insights into the structural requirements for preferential CO_2 reduction and the formation of C2

products. In addition, this synthetic approach may prove useful for preparing additional electrocatalysts for CO_2 reduction.

Embodiments of Implementation

[0056] To facilitate understanding of the invention, FIG. 8 is a high level flow chart of an embodiment of the invention. In this embodiment, a cathode with a catalyst metal is provided (step 804). A metal oxide coating is formed on the catalyst metal (step 808). The metal oxide coating and the catalyst metal form a metal and metal oxide coating, which may comprise a metal oxide coating over a metal coating or a single coating with both metal oxide particles and metal particles. An anode is spaced apart from the cathode (step 812). An ionic transport is provided between the anode and cathode (step 816). The cathode is exposed to CO_2 and H_2O (step 820). The anode is exposed to H_2O (step 824). A voltage is provided between the cathode and anode (step 828). The voltage causes CO_2 and H_2O to be reduced to CO, H_2 , and O_2 . The CO and H_2 may be converted to hydrocarbon or alcohol products.

[0057] In a specific embodiment of the invention, the cathode is formed by providing a conductive substrate (step 804) with a catalyst metal coating (step 808). FIG. 9A is an enlarged cross-sectional view of part of a conductive substrate 904 with a metal coating 908, forming part of a cathode 912. In this example, the conductive substrate 904 is steel. The metal coating 908 is copper. The conductive substrate may be in the form of a net over which the metal coating is applied. In other embodiments, the conductive substrate and metal coating may be a single piece of the same material, such as a copper wire. In such a case, the metal coating may be considered an outer layer of the metal substrate.

[0058] A metal oxide coating is formed on the catalyst metal (step 808). FIG. 9B shows the part of the cathode 912 after the metal oxide coating 916 is formed. In this example, part of the copper catalyst metal coating 908 is formed into copper oxide by heating the cathode to at least 300°C . for at least 15 minutes. Preferably, the metal oxide coating is thicker than a native oxide layer. For example, the metal oxide coating has a thickness of at least twice the thickness of a native metal oxide layer. More preferably, the metal oxide coating is at least 50 nm thick. In other embodiments, the metal oxide coating 916 may be provided by a deposition process to deposit the metal oxide coating on the catalyst metal coating. In this example the copper catalyst metal coating 908 and the metal oxide coating 916 form a metal and metal oxide coating. In other embodiment, metal particles and metal oxide particles may form a single layer to form the metal and metal oxide coating.

[0059] In some embodiments, some or all of the native metal oxide layer may be reduced before or during usage as a cathode. In the specification and claims, the term “oxidized cathode” will apply to a cathode on which an oxide layer is formed on the cathode by a process that increases the thickness of the metal oxide beyond that of a native metal oxide, whether the metal oxide coating remains or is subsequently reduced. Therefore the oxidized cathode is a cathode with an oxidized cathode layer, which is a metal and metal oxide coating where the metal oxide either remains or is reduced back to metal, and wherein the metal oxide is at least twice as thick as native metal oxide.

[0060] An anode is spaced apart from the cathode (step 812). FIG. 10 is a schematic view of an electrolyzer 1000 that

may be used in an embodiment of the invention. An anode is formed by a conductive anode substrate **1004** covered with an anode material **1008**. In this example, the anode material **1008** is nickel. An anode electrolyte compartment **1012** is adjacent to the anode and holds an anode electrolyte. The anode electrolyte is provided from an anode electrolyte source **1016**, which may continuously circulate anode electrolyte through the anode electrolyte compartment **1012**. A cathode electrolyte compartment **1020** holds a cathode electrolyte. The cathode electrolyte is provided from a cathode electrolyte source **1024**, which may continuously circulate cathode electrolyte through the cathode electrolyte compartment **1020**. Alternatively, the cathode electrolyte may flow to a tank where the solution-phase products are collected. A separator **1028** is placed between the anode electrolyte compartment **1012** and the cathode electrolyte compartment **1020**. The separator **1028** may be a porous frit or membrane that may allow certain ions to pass through the separator **1028**. As described above, a cathode comprising a conductive substrate **904** with an oxidized cathode layer **1032** forms a cathode adjacent to the cathode electrolyte compartment **1020**. In this embodiment, a gas chamber **1036** is placed on the backside of the cathode. A CO₂ source **1040** provides a flow of CO₂ into the gas chamber **1036**. A product collector **1044** collects gas-phase products and unused CO₂ from the gas chamber **1036**. Product in the product collector **1044** may be isolated and the remaining CO₂ may be recycled back to the CO₂ source **1040**. A voltage source **1048**, such as a battery, provides a voltage between the anode and cathode.

[0061] In operation, the anode electrolyte source **1016** flows electrolyte through the anode electrolyte compartment **1012**. The cathode electrolyte source **1024** flows electrolyte through the cathode electrolyte compartment **1020**. CO₂ is flowed from the CO₂ source **1040** into the gas chamber **1036**. The voltage source **1048** applies a positive voltage to the anode substrate **1004** and a negative voltage to the cathode substrate **904** with the anode connected to a positive terminal and the cathode connected to a negative terminal. The process provides electrolysis of the CO₂. Various chemical reactions may occur during the electrolysis of CO₂, depending on the metal cathode and other factors. One chemical reaction is $\text{CO}_2 + \text{H}_2\text{O} \rightarrow \text{H}_2 + \text{O}_2$. Other chemical reactions provide products of HCO₂H, CH₃OH or C₂H₄. In a preferred embodiment, the product collector **1044** provides the product to another system that converts CO, O₂, and H₂ and possibly other products to methanol or some other fuel or usable chemical.

[0062] It has been unexpectedly found that by providing a metal oxide layer on a cathode that is thicker than the native oxide layer and subsequently reducing the metal oxide layer, the reduction of CO₂ is improved. Without being bound by theory, it is believed that the reduction of the thick metal oxide layer results in metal particles that have unique structures that result in improved CO₂ reduction, however, the reason for the improvement is currently unknown. It has also been unexpectedly found that for some cathodes having a metal and metal oxide interface improves CO₂ reduction. Preferably, the metal and metal oxide use the same metal material. However, in an embodiment using cerium oxide, the metal is something other than cerium such as tin or copper. Since cerium would turn to cerium oxide during electrolysis, tin is used to provide a native metal for an enhanced metal oxide metal interface, which provides improved CO₂ reduction.

[0063] As demonstrated above, copper cathodes that are annealed at 130° C. to grow the oxidation layer do not provide the desired improvement. Annealing copper at 300° C. provides some improvement. It has been found that annealing copper at over 500° C. provides the preferred improvement. Anodization at a constant potential for several hours can also be used to obtain a thick Cu₂O layer on Cu and results in improved CO₂ reduction.

[0064] In the case of some metals such as gold, neither annealing in air or O₂ or anodization at a constant potential is effective for preparing a thick oxide layer. Instead, a square wave potential routine is preferred to obtain the metal oxide layer. In the case of gold, a thick, hydrous Au₂O₃ layer can be formed on the Au electrode by applying a square wave potential alternating between 2.7 V and 0.45 V vs Hg/HgSO₄ at a frequency of 1 kHz for 30-60 min. Subsequent reduction of this Au₂O₃ layer results in a Au electrode with greatly improved CO₂ reduction activity and resistance to catalyst deactivation. Similarly, growth of a silver oxide on silver electrodes by application of a square wave potential routine, followed by electrochemical reduction, results in an Ag electrode with greatly improved CO₂ reduction activity and resistance to catalyst deactivation.

[0065] FIG. 11 is a high level flow chart of another embodiment of the invention. In this embodiment, a cathode with a catalyst metal is provided (step **1104**). A metal oxide coating is formed on the catalyst metal (step **1108**). The metal oxide coating and the catalyst metal form a metal and metal oxide coating, which may comprise a metal oxide coating over a metal coating or a single coating with both metal oxide particles and metal particles. An anode is spaced apart from the cathode (step **1112**). An ionic transport is provided between the anode and cathode (step **1116**). The cathode is exposed to CO and H₂O (step **1120**). The anode is exposed to H₂O (step **1124**). A voltage is provided between the cathode and anode (step **1128**). The voltage causes CO and H₂O to be reduced to CH₃CH₂OH.

[0066] In a specific embodiment of the invention, the cathode is formed by providing a conductive substrate (step **1104**) with a catalyst metal coating (step **1108**). In this example, the conductive substrate is steel. The metal coating is copper. The conductive substrate may be in the form of a net over which the metal coating is applied. In other embodiments, the conductive substrate and metal coating may be a single piece of the same material, such as a copper wire. In such a case, the metal coating may be considered an outer layer of the metal substrate.

[0067] A metal oxide coating is formed on the catalyst metal (step **1108**). In this example, part of the copper catalyst metal coating is formed into copper oxide by heating the cathode to at least 300° C. for at least 15 minutes. Preferably, the metal oxide coating is thicker than a native oxide layer. For example, the metal oxide coating has a thickness of at least twice the thickness of a native metal oxide layer. More preferably, the metal oxide coating is at least 50 nm thick. In this example the copper catalyst metal coating and the metal oxide coating form a metal and metal oxide coating.

[0068] An anode is spaced apart from the cathode (step **1112**). FIG. 12 is a schematic view of an electrolyzer **1200** that may be used in an embodiment of the invention. An anode is formed by a conductive anode substrate **1204** covered with an anode material **1208**. In this example, the anode material **1208** is nickel. An anode electrolyte compartment **1212** is adjacent to the anode and holds an anode electrolyte. The

anode electrolyte is provided from an anode electrolyte source **1216**, which may continuously circulate anode electrolyte through the anode electrolyte compartment **1212**. A cathode electrolyte compartment **1220** holds a cathode electrolyte. The cathode electrolyte is provided from a cathode electrolyte source **1224**, which may continuously circulate cathode electrolyte through the cathode electrolyte compartment **1220**. In this embodiment, the cathode electrolyte flows to a product collector **1244** where the solution-phase products are collected. A separator **1228** is placed between the anode electrolyte compartment **1212** and the cathode electrolyte compartment **1220**. The separator **1228** may be a porous fit or membrane that may allow certain ions to pass through the separator **1228**. As described above, a cathode comprising a conductive substrate **1230** with an oxidized cathode layer **1232** forms a cathode adjacent to the cathode electrolyte compartment **1220**. In this embodiment, a gas chamber **1236** is placed on the backside of the cathode. A CO source **1240** provides a flow of CO into the gas chamber **1236**. The product collector **1244** collects products and unused CO from the gas chamber **1236**. Product in the product collector **1244** may be isolated and the remaining CO may be recycled back to the CO source **1240**. A voltage source **1248**, such as a battery, provides a voltage between the anode and cathode.

[0069] In operation, the anode electrolyte source **1216** flows electrolyte through the anode electrolyte compartment **1212**. The cathode electrolyte source **1224** flows electrolyte through the cathode electrolyte compartment **1220**. In this example, the electrolyte is KOH in an aqueous solution. CO is flowed from the CO source **1240** into the gas chamber **1236**. The voltage source **1248** applies a positive voltage to the anode substrate **1204** and a negative voltage to the cathode substrate **1230** with the anode connected to a positive terminal and the cathode connected to a negative terminal. The process provides electrolysis of the CO. Various chemical reactions may occur during the electrolysis of CO, depending on the metal cathode and other factors. If the reduction uses an acidic aqueous solution for ion transport, in one embodiment, the following reaction occurs: $2\text{CO} + 8\text{e}^- + 8\text{H}^+ \rightarrow \text{CH}_3\text{CH}_2\text{OH} + \text{H}_2\text{O}$. If the reduction uses a basic aqueous solution for ion transport, in another embodiment, the following reaction occurs: $2\text{CO} + 8\text{e}^- + 7\text{H}_2\text{O} \rightarrow \text{CH}_3\text{CH}_2\text{OH} + 8\text{OH}^-$. Since the product is $\text{CH}_3\text{CH}_2\text{OH}$, may be produced in liquid phase, the product may diffuse through the conductive substrate **1230** and the oxidized cathode layer **1232** to the cathode electrolyte compartment **1220**. In such a case, the product collector **1244** would need to remove the product from the cathode electrolyte.

[0070] In one embodiment, the product collector **1044** for a CO_2 reduction system may provide CO for the CO source **1240** for the CO reduction system. In another embodiment, another source of CO may be used. In another embodiment, a source of a mixture of CO and CO_2 may provide both CO and CO_2 to a reduction system. In some embodiments, the pressure of the CO from the CO source **1240** is provided at a pressure greater than 1 atm. The higher pressure increases the solubility of CO in an aqueous solution. The use of an oxide-derived Cu catalyst in embodiments of the invention proved CO reduction with a high energetic efficiency without requiring H_2 . In another embodiment of the invention, CO is converted to acetate according to the equation $2\text{CO} + 4\text{e}^- + 3\text{H}^+ \rightarrow \text{CH}_3\text{CO}_2^-$. In another embodiment of the invention, CO is converted to ethylene according to the equation $2\text{CO} + 8\text{e}^- + 8\text{H}^+ \rightarrow \text{C}_2\text{H}_4 + 2\text{H}_2\text{O}$. In other embodiments, the electrolytic

reduction reduces CO to other hydrocarbons or alcohols. In other embodiments, the electrolytic reduction reduces CO_2 to hydrocarbons or alcohols.

[0071] While this invention has been described in terms of several preferred embodiments, there are alterations, permutations, modifications and various substitute equivalents, which fall within the scope of this invention. It should also be noted that there are many alternative ways of implementing the methods and apparatuses of the present invention. It is therefore intended that the following appended claims be interpreted as including all such alterations, permutations, modifications, and various substitute equivalents as fall within the true spirit and scope of the present invention.

What is claimed is:

1. A method for electrochemically reducing CO, comprising:
 - providing a cathode, wherein the cathode comprises a conductive substrate with a catalyst of a metal and a metal oxide based coating on a side of the cathode;
 - providing an anode spaced apart from the cathode;
 - providing an ionic transport between the anode and cathode;
 - exposing the cathode to CO and H_2O ;
 - exposing the anode to H_2O ; and
 - providing a voltage between the cathode and anode.
2. The method, as recited in claim 1, wherein the metal oxide is copper oxide.
3. The method, as recited in claim 2, wherein the metal oxide is thicker than the native oxide.
4. The method, as recited in claim 3, wherein the providing the cathode comprises:
 - providing a conductive substrate with a metal coating; and
 - providing on the conductive substrate a metal oxide coating that is thicker than a native oxide layer by either annealing the metal coating, electrochemically oxidizing the metal coating, chemically oxidizing the metal coating or depositing a metal oxide layer.
5. The method, as recited in claim 4, further comprising reducing metal oxide in the metal and metal oxide based coating to the metal 0 oxidation state.
6. The method, as recited in claim 5, where the metal oxide in the metal and metal oxide based coating has a thickness that is greater than 50 nm.
7. The method, as recited in claim 1, wherein the metal oxide and metal are of the same metal material.
8. The method, as recited in claim 1, wherein the metal and metal oxide containing coating provide a metal and metal oxide interface.
9. The method, as recited in claim 1, wherein the exposing the cathode to CO and H_2O , comprises:
 - exposing a first side of the cathode to H_2O ; and
 - flowing CO past a second side of the cathode.
10. The method, as recited in claim 1, wherein the providing the cathode, comprises:
 - providing a conductive substrate with a metal coating; and
 - applying an anodic square wave potential to the metal coating to form an oxide layer.
11. The method, as recited in claim 1, wherein the metal coating is copper or copper alloy.
12. The method, as recited in claim 1, wherein the ionic transport is an aqueous basic solution.
13. A method for electrochemically reducing CO, comprising:

providing on a cathode a coating formed by heating a metal layer of the cathode in air, electrochemically oxidizing the metal layer of the cathode, chemically oxidizing the metal layer or by a metal oxide deposition to form a metal and metal oxide interface;
 providing an anode spaced apart from the cathode;
 providing an ionic transport between the anode and cathode;
 exposing the coating to CO and H₂O;
 exposing the anode to H₂O; and
 providing a voltage between the cathode and anode.

14. The method, as recited in claim **13**, wherein the cathode is copper and the coating is formed by heating the cathode to a temperature of at least 500° C. for at least 15 minutes.

15. The method, as recited in claim **13**, wherein the cathode is copper and the coating is formed by heating the cathode to a temperature of at least 300° C. for at least 15 minutes.

16. The method, as recited in claim **13**, further comprising reducing the metal oxide to metal.

17. The method, as recited in claim **13**, where the metal oxide has a thickness that is greater than 50 nm.

18. The method, as recited in claim **13**, where the metal oxide has a thickness that is greater than twice a thickness of a native oxide layer.

19. The method, as recited in claim **13**, wherein the providing on a cathode a coating, comprises applying an anodic square wave potential to the metal layer to form an oxide layer.

20. The method, as recited in claim **13**, wherein the metal layer is copper or copper alloy.

21. The method, as recited in claim **13**, wherein the metal oxide is copper oxide.

22. The method, as recited in claim **13**, wherein the ionic transport is an aqueous basic solution.

23. An apparatus, for electrochemically reducing CO, comprising:

an anode;

an oxidized cathode spaced apart from the anode;

a chamber for exposing the anode and oxidized cathode to at least one electrolyte adjacent to the anode and oxidized cathode;

a gas chamber for exposing the oxidized cathode to CO adjacent to the oxidized cathode; and

a CO source for providing CO to the gas chamber, connected to the gas chamber.

24. The apparatus, as recited in claim **23**, wherein the oxidized cathode comprises:

a conductive substrate; and

an oxidized layer over the conductive substrate.

25. The apparatus, as recited in claim **24**, wherein the oxidized layer, comprises:

a metal layer formed over the conductive substrate; and

a metal oxide layer formed over the conductive substrate and forming a metal layer metal oxide layer interface.

26. The apparatus, as recited in claim **25**, wherein the oxidized layer is subsequently reduced.

27. The apparatus, as recited in claim **23**, wherein the oxidized cathode comprises a metal layer that has been oxidized using an anodic square wave potential.

28. The apparatus, as recited in claim **23**, wherein the metal layer is copper or copper alloy.

29. The apparatus, as recited in claim **23**, wherein the metal oxide layer is copper oxide.

* * * * *